bioRxiv preprint doi: https://doi.org/10.1101/288480; this version posted March 25, 2018. The copyright holder for this preprint (which was not certified by peer review) is the author/funder. All rights reserved. No reuse allowed without permission.

Transcriptional and electrophysiological aberrations in an induced pluripotent stem cell-derived model of spinocerebellar ataxia type 7

LM Watson[1,2†], DC Smith[1,2†], JV Raimondo[2,3,4†], RJ Burman[2,3,4], R Ballo[4], J Scholefield[5], L Tyers[4], SA Cowley[6], MJA Wood[1,7], SH Kidson[2,4], LJ Greenberg[1,2*]

[1]Division of Human Genetics, Department of Pathology, Faculty of Health Sciences, University of Cape Town, Cape Town, South Africa

[2]Institute of Infectious Disease and Molecular Medicine, Faculty of Health Sciences, University of Cape Town, Cape Town, South Africa

[3]Neuroscience Institute, Faculty of Health Sciences, University of Cape Town, Cape Town, South Africa

[4]Division of Cell Biology, Department of Human Biology, Faculty of Health Sciences, University of Cape Town, Cape Town, South Africa

[5]Gene Expression & Biophysics Group, Synthetic Biology ERA, CSIR Biosciences, Pretoria, South Africa

[6]Sir William Dunn School of Pathology, University of Oxford, Oxford, United Kingdom

[7]Department of Physiology, Anatomy and Genetics, University of Oxford, Oxford, United Kingdom

[†]These authors contributed equally to this work.

***Correspondence:** LJ Greenberg: jacquie.greenberg@uct.ac.za

Keywords: cellular electrophysiology, induced pluripotent stem cells, transcriptomics, spinocerebellar ataxia type 7

Abstract

Spinocerebellar ataxia type 7 (SCA7) is an inherited neurodegenerative disease that is characterised by ataxia and visual loss. It results from a degeneration of cerebellar Purkinje neurons and retinal photoreceptors caused by a polyglutamine repeat expansion in the ATXN7 gene, a component of the STAGA transcription co-activator complex. As with many neurodegenerative diseases, studies of pathogenesis have been hindered by a lack of disease-relevant models. To this end, we have generated the first induced pluripotent stem cells (iPSCs) from South African SCA7 patients, where the disease occurs at an unusually high frequency as a result of a founder effect. These iPSCs were capable of differentiation into neural and retinal cells, and showed evidence of a transcriptional phenotype affecting components of STAGA (*ATXN7* and *KAT2A*) and the heat shock protein pathway (*DNAJA1* and *HSP70*). Functionally, SCA7 iPSC-derived neurons exhibited more negative resting membrane potentials and increased input resistance compared to controls, suggesting reduced excitability in response to synaptic input. These results provide the first evidence of a disease phenotype in SCA7 iPSC-derived cells, establishing a valuable model for the study of neurodegenerative diseases and the development of population-specific therapies.

bioRxiv preprint doi: https://doi.org/10.1101/288480; this version posted March 25, 2018. The copyright holder for this preprint (which was not certified by peer review) is the author/funder. All rights reserved. No reuse allowed without permission.

1. Introduction

Spinocerebellar ataxia type 7 (SCA7) is an inherited neurodegenerative disease caused by a CAG repeat expansion in the *ATXN7* gene. Since the translation of this CAG repeat leads to an expanded polyglutamine (polyQ) tract within the resultant protein, SCA7 is classified as a polyQ-repeat disorder. Other diseases with a similar pathophysiology include five different SCAs (SCA 1, 2, 3, 6 and 17), as well as Huntington disease, dentatorubral-pallidoluysian atrophy and spinal bulbar muscular atrophy (Orr and Zoghbi, 2007).

Clinically, SCA7 patients present with ataxia, dysarthria and visual loss. This is caused by a selective degeneration of cerebellar Purkinje neurons and retinal photoreceptors (Gouw et al., 1994). Symptoms progressively worsen over a period of 10 to 30 years, leading ultimately to brainstem dysfunction, blindness, physical disability and death.

The mechanism by which a polyQ expansion within the ubiquitously expressed ATXN7 protein leads to the selective degeneration of Purkinje neurons and photoreceptors remains to be fully elucidated. ATXN7 is known to be a component of the mammalian transcription co-activator complex, STAGA (SPT3-TAF9-ADA-GCN5 acetyltransferase) (Garden and La Spada, 2008), and has been shown to facilitate interaction between STAGA and the cone-rod homeobox (CRX) transactivator of photoreceptor genes, linking the function of ATXN7 with the retinal phenotype observed in SCA7 patients (Palhan et al., 2005). In neuronal cells, several studies have highlighted the role of transcriptional aberrations in the dysfunction that precedes the onset of disease symptoms (Palhan et al., 2005, Ström et al., 2005, Abou-Sleymane et al., 2006, Garden and La Spada, 2008, Chou et al., 2010,). These gene expression changes may arise either directly from alterations in transcriptional regulation by mutant ATXN7, or indirectly, as a consequence of a generalised cellular response to the presence of mutant ATXN7.

As with many neurodegenerative conditions, research into the molecular pathogenesis of SCA7 has been hindered by a lack of suitable models of human disease progression. This is particularly relevant in cases where the genomic context of the mutation may have an impact on gene function and might prove useful for therapeutic development. SCA7 occurs at an unusually high frequency in the South African population as a result of a founder effect in patients of Black African ethnic origin (Smith et al., 2012, Smith et al., 2016). South African SCA7 patients also display a unique phenomenon – a single nucleotide polymorphism (SNP) within *ATXN7* (rs3774729), which is linked to the mutation in all patients studied to date (Greenberg et al., 2006). Approximately 43% of these individuals are heterozygous for the polymorphism, allowing for allelic discrimination, and providing an ideal target for developing an allele-specific silencing therapy. Recently, this haplotype has been shown to extend into other Southern African populations, suggesting that such a therapy may be more widely ****applicable than was first thought (Smith et al., 2015). We have previously demonstrated the efficacy of an allele-specific RNAi treatment in an over-expression cell model of SCA7 (Scholefield et al., 2009), as well as in SCA7 patient fibroblasts (Scholefield et al., 2014). Disease-relevant cell lines generated from these patients are thus of vital importance in the understanding of disease pathogenesis and the development of therapies, as they carry the patient's full genomic sequence, including SNPs which may be used as targets for gene silencing.

In this study, we have generated and characterised multiple induced pluripotent stem cell (iPSC) lines from two South African SCA7 patients and an unaffected, related control. The generation of iPSCs involves reprogramming somatic cells to a pluripotent state by means of viral transduction with the pluripotency genes *OCT4*, *SOX2*, *KLF4* and *c-MYC* (Takahashi and Yamanaka, 2006, Takahashi et al.,

bioRxiv preprint doi: https://doi.org/10.1101/288480; this version posted March 25, 2018. The copyright holder for this preprint (which was not certified by peer review) is the author/funder. All rights reserved. No reuse allowed without permission.

2007). Importantly, iPSCs can then be differentiated into any tissue of the body through treatment with specific growth factors, making them a useful starting point for the generation of disease-relevant cell models, particularly in neurodegenerative diseases, where primary CNS cultures may only be obtained using invasive methods. We have successfully differentiated SCA7 patient and control iPSCs into cells expressing markers associated with retinal photoreceptors, neural progenitors and neurons. Furthermore, we have obtained preliminary evidence for a disease phenotype in these cells, in the form of pathogenically relevant gene expression changes and alterations in intrinsic neuronal properties. These cells may thus provide a highly relevant model in which to screen potential therapeutic modalities, by monitoring the effect of such therapies on disease manifestations *in vitro*.

2. Methods

Ethics approval and patient recruitment

Ethics approval for the study was granted by the University of Cape Town (UCT) Faculty of Health Sciences Human Research Ethics Committee (HREC REF. 380/2009 and 434/2011), and was renewed annually, incorporating amendments to the project protocol where necessary. All methods were carried out in accordance with the guidelines approved by the Ethics Committee. Participants were recruited from the Neurogenetics clinic at Groote Schuur Hospital in Cape Town. Informed consent was obtained from all participants prior to their enrolment in the study.

Establishment of primary fibroblast cultures

Primary fibroblast cultures were established from punch skin biopsies taken from the inner forearm of two unrelated SCA7 patients (P1 and P2) and an unaffected control individual (C1, sibling of P2) who had consented to participate in the study, as previously described (Freshney, 2000). CAG genotypes and ages at diagnosis and biopsy are reflected in **Table S-1.1**.

Generation and characterisation of patient-derived iPSCs

Reprogramming of dermal fibroblasts into iPSCs was achieved through the introduction of Sendai virus vectors (SeVdp) containing *OCT4, SOX2, KLF4* and *c-MYC* as previously described (Nishimura et al., 2011, Nakanishi and Otsu, 2012). The expression of pluripotency markers OCT4 and TRA-1-60, as well as silencing of the reprogramming Sendai virus, were confirmed by immunocytochemistry (antibodies listed in **Table S-1.2**). The expression of selected pluripotency genes (*OCT4, SOX2, NANOG*) was determined by quantitative PCR (see below). Genomic integrity was assessed by means of karyotype analysis (G-banding). To confirm the iPSC lines' capacity to differentiate into the three embryonic germ layers, *in vitro* differentiation via embryoid body formation was performed as previously described (Martl et al., 2013).

Neural differentiation and characterisation

Differentiation of iPSCs into neural precursors was performed by treatment of iPSCs with 3µM glycogen synthase kinase 3 (GSK3) inhibitor (CHIR99021) and 2µM TGFβ inhibitor (SB431542) as previously described (Li et al., 2011). For neuronal differentiation, neural precursors were seeded at a density of 150 000 cells/well onto a Matrigel-coated six-well plate in neural induction medium (Li et al., 2011). After two days, medium was changed to neuronal differentiation medium supplemented with N2, B27, 300ng/ml cyclic AMP (Sigma), 0.2mM ascorbic acid (Sigma), 10ng/ml BDNF (Peprotech) and 10ng/ml GDNF (Peprotech) and cells were maintained in culture for 14 to 21 days.

bioRxiv preprint doi: https://doi.org/10.1101/288480; this version posted March 25, 2018. The copyright holder for this preprint (which was not certified by peer review) is the author/funder. All rights reserved. No reuse allowed without permission.

Characterisation was performed by immunocytochemistry and qPCR (for antibodies and primers, see **Tables S-1.2** and **S-1.3**).

Electrophysiology

Neurons maintained on glass cover slips were removed from the incubator and rapidly transported to the recording chamber of a Zeiss Axioskop Upright Microscope (Zeiss). Electrophysiological recordings were made in neuronal differentiation medium at room temperature and were restricted to the first 5 hours following cell removal from the incubator environment. Patch pipettes of 13-20 MOhm tip resistance were pulled from filamental borosilicate glass capillaries (2.00 mm outer diameter, 1.58 mm inner diameter, Hilgenberg), using a horizontal puller (Model P-1000, Sutter). The pipettes were filled with an internal solution containing (in mM): K-gluconate (126); KCl (4); Na 2 ATP (4); NaGTP (0.3); Na 2 -phosphocreatinine (10) and HEPES (10). Osmolarity was adjusted to between 290 and 300 mOsM and the pH was adjusted to between 7.38 and 7.42 with KOH. Cells were visualised using a 40x water-immersion objective (Zeiss). Digital images were obtained using a CCD camera (VX55, TILL Photonics). Individual cells were selected for recordings based on a small round or ovoid cell body (diameters, 5–10 μm) and typically two or more extended processes. Recordings were made in current clamp and voltage clamp mode using an Axopatch 200B amplifier (Molecular Devices). Data acquisition was performed through an ITC-1600 board (Instrutech) connected to a PC running a custom-written routine (PulseQ) under IGOR Pro (Wavemetrics). Analysis was performed using custom-written scripts in MATLAB (Mathworks).

Retinal differentiation and characterisation

Differentiation into retinal photoreceptors was performed as previously described (Boucherie et al., 2013), using iPSCs cultured in feeder-free conditions on Matrigel in mTESR™ medium. The cells were dissociated enzymatically and plated onto Matrigel-covered dishes in neural differentiation medium containing N2 and B27 supplements (Life Technologies). After settling for an hour, adhered cells were covered in a 2% Matrigel solution. The following day the medium was replaced with neural differentiation medium without Matrigel, and cells were fed with fresh medium every second day. From day 10 the medium was supplemented with 3nM recombinant SHH (R&D Systems), 50ng/μl acidic fibroblast growth factor (aFGF) (R&D Systems), 10ng/μl basic fibroblast growth factor (bFGF) (Miltenyi), 1mM taurine and 500nM retinoic acid (both Sigma Aldrich). Characterisation was performed by immunocytochemistry and qPCR (for antibodies and primers, see **Tables S-1.2 and S-1.3**).

DNA and RNA isolation, cDNA synthesis

DNA extraction from cultured cells was performed using the QIAGEN DNeasy Blood and Tissue Kit. RNA was isolated from cultured cells using the QIAGEN RNeasy Plus Mini Kit. Synthesis of cDNA was performed using the Applied Biosystems High Capacity cDNA Reverse Transcription Kit (Life Technologies) using 500ng-1μg template RNA.

Real-time quantitative PCR

Real-time quantitative PCR (qPCR) was performed on the BioRad CFX96 Real-Time PCR System, using the Power SYBR Green PCR Master Mix (Applied Biosystems), according to manufacturer's instructions. Primers (**Table S-1.2**) were obtained from PrimerDesign Ltd, Integrated DNA Technologies (IDT), or Sigma-Aldrich.

bioRxiv preprint doi: https://doi.org/10.1101/288480; this version posted March 25, 2018. The copyright holder for this preprint (which was not certified by peer review) is the author/funder. All rights reserved. No reuse allowed without permission.

Relative quantities of target mRNA were determined using the relative standard curve method (Larionov et al., 2005). Standard curves were prepared for each primer pair, from serial dilutions of pooled sample cDNA. Universal cycling conditions were used (95°C for 10min, followed by 40 cycles of 95°C for 15 seconds and 60°C for 1min). PCRs were performed in technical triplicate, on at least two biological replicates, and results were analysed using the BioRad CFX Manager software (v3.1). Gene of interest expression was normalised to *beta actin* (*ACTB*) expression in each case. The design and reporting of qPCR experiments aimed to comply with the Minimum Information for publication of Quantitative real-time PCR Experiments guidelines (Taylor et al., 2006, Bustin et al., 2009) wherever possible. Statistical analysis was performed using the Students' t-test (two-tailed, assuming unequal variances). Significance was defined as $p<0.05$.

CAG repeat length determination

The length of the disease-causing CAG repeat in *ATXN7* was determined from DNA by means of polymerase chain reaction (PCR) and automated fluorescent genotyping. The PCR reaction mix consisted of 0.4µM each, forward and reverse primer (**Table S-1.1**), 0.6units of GoTaq DNA polymerase (Promega), 100ng of DNA, and Failsafe buffer J (Epicentre Biotechnologies) at a final concentration of 1X, made up to a final reaction volume of 10µl. Cycling conditions were as follows: 95°C for 5min; followed by 30 cycles of 95°C for 30 seconds, 53°C for 6 seconds and 72°C for 40 seconds; and a final elongation step at 72°C for 7min. Automated fluorescent genotyping was performed using the ABI 3130*xl* Genetic Analyzer (Applied Biosystems).

The length of the CAG repeat [$(CAG)_n$] was approximated using the following equation, adapted from (Dorschner et al., 2002): n = (0.3063 x Length of major PCR product in base pairs) – 76.475bp. The major PCR product was defined as the product generating the highest fluorescent peak, as detected using the ABI 3130*xl* Genetic Analyzer.

3. Results

Generation and characterisation of iPSCs

Following Sendai virus-mediated reprogramming, iPSC colonies with the correct morphology (flat, with distinct borders, containing tightly packed cells with a high nucleus-to-cytoplasm ratio) appeared within three to four weeks (**Figure 1a**). These colonies were manually picked and clonally expanded in separate dishes on a feeder layer of inactivated mouse embryonic fibroblasts. Three SCA7 patient iPSC lines and two control lines (representing two affected individuals and a single related, unaffected control) were successfully generated and characterised (**Table S-1.1**).
Immunocytochemical analysis of SCA7 patient and control iPSC lines revealed iPSC colonies with distinct nuclear staining for the pluripotency transcription factor, OCT4, compared to the surrounding mouse embryonic feeder fibroblasts (**Figure 1b**). The iPSC colonies also stained positive for the embryonic stem cell surface marker TRA-1-60 (**Figure 1b**).
The expression of pluripotency markers was further confirmed by qPCR. All five iPSC lines expressed high levels of *OCT4, SOX2* and *NANOG*, standard markers of pluripotency (**Figure 1c**), compared to donor fibroblasts or cells that had been subjected to retinal or neuronal differentiation. The expression levels of *SOX2* and *NANOG* were similar across the five iPSC lines, but lines P2b and C1b showed lower levels of *OCT4* expression compared to the remaining three lines (although still significantly higher than differentiated fibroblasts and retinal cells).
Co-staining of all iPSC lines with primary antibodies against OCT4 and the nucleocapsid protein of the virus (anti-NP) showed little or no evidence of NP staining in the OCT4-positive pluripotent cells

bioRxiv preprint doi: https://doi.org/10.1101/288480; this version posted March 25, 2018. The copyright holder for this preprint (which was not certified by peer review) is the author/funder. All rights reserved. No reuse allowed without permission.

(**Figure 1d**, bottom panel), compared to intense cytoplasmic staining in newly infected fibroblasts (**Figure 1d**, top panel). This indicated that the Sendai virus had been effectively silenced, and that the iPSCs had achieved self-regulating pluripotency. All lines were assessed after passage 8.

In vitro embryoid body-mediated differentiation confirmed the ability of all five lines to differentiate into the three embryonic germ layers, staining positive for forkhead box A2 (FOXA2) or alpha-fetoprotein (AFP) (endoderm); sarcomeric alpha actinin (ASA) or smooth muscle actin (SMA) (mesoderm); and glial fibrillary acidic protein (GFAP) or βIII-tubulin (ectoderm) (**Figure 1e**).

Karyotyping using standard G-banding analysis revealed no gross structural abnormalities, when iPSC lines were compared to the fibroblasts from which they had been derived (**Figure S-1.1**).

Neural differentiation of iPSCs

SCA7 patient and control iPSCs generated neural precursor cells (NPCs) at comparable efficiencies, when cultured in neural induction medium supplemented with SB431542 (TGFβ inhibitor) and CHIR99021 (GSK3 inhibitor), with 100% of the cells expressing the early neural marker Nestin, after five passages (**Figure 2a**). The cells also stained positive for the disease-causing protein, ATXN7 (**Figure 2b**), and demonstrated repression of the pluripotency gene *OCT4*, and upregulation of the early neural gene *PAX6* (**Figure 2c**).

After culture for 14 days in neuronal differentiation medium containing N2/B27 supplement, cAMP ascorbic acid, BDNF and GDNF (Li et al., 2011), both SCA7 patient and control NPCs stained positive for the neuronal marker βIII-Tubulin, and showed robust, diffuse nuclear localisation of the disease-causing protein, ATXN7 (**Figure 2d**). A subset of cells (approximately 1.8%) stained positive for gamma-aminobutyric acid (GABA), although the proportion of GABAergic neurons did not appear to vary between SCA7 patients and controls (**Figure 2d**). No obvious differences in morphology were observed when comparing neurons derived from SCA7 patient iPSCs with those derived from controls.

Cells were assayed for physiological properties between 14 and 23 days post induction of neuronal differentiation. Cells were targeted for whole-cell recordings based on their morphological properties. This included a small round or ovoid cell body with diameters between 5–10 μm and typically two or more extended processes (see **Figure 3a**). Following the attainment of a whole-cell patch, current pulses of between 0 and 10 pA were applied. Individual cells displayed four general types of spiking responses: a purely passive (**Figure 3a**), abortive spike (**Figure 3b**), single spike (**Figure 3c**) and recurrent spiking response (**Figure 3d**). These spiking properties are similar to those observed in acute human fetal brain slices (Moore et al., 2009), hESC-derived neurons (Perrier et al., 2004; Vazin et al., 2009; Belinsky et al., 2011) and iPSC-derived neurons (Belinsky et al., 2014). A postmitotic neuron matures by inserting voltage-gated channels into its plasma membrane (Moody and Bosma, 2005). Therefore the spiking response of a cell to current injection can be used to determine the maturation stage of a differentiating neuron: passive (least mature) → abortive spike → single spike → recurrent spikes (most mature).

Spiking responses were collected in current-clamp mode from cells derived from four separate iPSC lines: two control lines C1a (n = 42) and C1b (n = 69), and two patient lines P1a (n = 44) and P2b (n = 72). Although the fraction of cells which fell into each spiking response category was significantly dependent on the iPSC line from which the cells were derived ($p<0.0001$, Chi-squared test), no trend could be discerned between control and patient lines (see **Figure 3e**). For example, the control line C1b had the most mature phenotype with the highest fraction of cells in the single spike and recurrent

bioRxiv preprint doi: https://doi.org/10.1101/288480; this version posted March 25, 2018. The copyright holder for this preprint (which was not certified by peer review) is the author/funder. All rights reserved. No reuse allowed without permission.

spiking categories whilst P2b demonstrated a relatively immature phenotype, with the majority of cells displaying spiking responses falling into the passive category. However, this difference was not corroborated by the other lines where the control line C1a displayed a less mature phenotype than patient line P1a. The maximum number of spikes that could be elicited following current injection was again significantly dependent on the cell line concerned. Mean values +/- SEM for each line were: C1a 0.5 +/- 0.1, C1b 1.3 +/- 0.2, P1a 1.0 +/- 0.3 and P2b 0.4 +/- 0.1 spikes, see **Figure 3f**, $p<0.0001$, ANOVA. However, no consistent trend could be observed between cells derived from control versus patient iPSC lines.

Next, we compared the resting membrane potential (Vm) of cells derived from each cell line. This parameter was significantly dependent on the iPSC line from which the cells were derived (see **Figure 3g**, $p = 0.0004$, ANOVA). The mean resting membrane potential +/- SEM for the C1a, C1b, P1a and P2b cell lines were -54.7 +/- 3.1, -57.0 +/- 1.7, -67.4 +/- 2.8 and -67.3 +/- 2.7 mV respectively. The control lines had significantly more depolarised resting membrane potentials as compared to patient derived cell lines ($p < 0.0001$, t-test).

We then determined the input resistance of each cell. A lower input resistance is associated with neurite outgrowth and increased numbers of ion channels inserted into the plasma membrane during the process of neuronal maturation. Once again, a cell's input resistance was significantly dependent on the cell line to which it belonged (see **Figure 3h**, $p = 0.0012$, ANOVA). Input resistance +/- SEM was 4987 +/- 421, 5484 +/- 243, 5979 +/- 513 and 7094 +/- 455 mΩ for the C1a, C1b, P1a and P2b cell lines respectively. Cells derived from patient lines had a significantly higher mean input resistance than cells from the control lines ($p = 0.0005$, t-test).

Following our assessment of the active and passive properties of cells described above, we then directly measured voltage-gated sodium and potassium currents in voltage-clamp mode (**Figure 4a**,**b** and **c**). As one would predict, the spiking properties of neurons are directly correlated with the size of their currents. Indeed we found a significant correlation between the maximum number of spikes that could be elicited in a cell and the size of its subsequently measured voltage-gated sodium and potassium currents (data not shown, $r = -0.62$ and 0.36 for voltage-gated sodium and potassium currents respectively, $p < 0.0001$ for both, Pearson correlation).

The maximum size of voltage-gated sodium currents and potassium currents measured in each cell (Max. I_{NA} and Max. I_K) was significantly dependent on the particular iPSC line concerned (see **Figure 4d** and **e**, $p < 0.0001$ in both cases, ANOVA). The mean Max. I_{NA} +/- SEM was -166.5 +/- 18.6, -277.1 +/- 23.0, -268.0 +/- 30.5 and -108.0 +/- 14.2 pA for the C1a, C1b, P1a and P2b cell lines. The mean Max. I_K +/- SEM was 180.1 +/- 16.5, 176 +/- 10.8, 222.5 +/- 19.3 and 105.7 +/- 8.0 pA for the C1a, C1b, P1a and P2b cell lines respectively. Similar to what was observed for the spiking responses, there was no consistent trend in the size of voltage-gated currents between cells derived from control as compared to iPSC lines.

Retinal differentiation of iPSCs

For the retinal differentiation of iPSCs, the Matrigel "sandwich" system facilitated a rapid self-organisation and differentiation of the pluripotent stem cells into structures containing cells morphologically indicative of columnar neuroepithelia (**Figure 5a**, first image). These structures lost their integrity from day 4-5, and cells spread into an adherent monolayer (**Figure 5a**, middle image). The gradual emergence of cells with a neuronal morphology was observed from day 10 to day 30, particularly in areas of low confluence (**Figure 5a**, last image). Following differentiation of patient

bioRxiv preprint doi: https://doi.org/10.1101/288480; this version posted March 25, 2018. The copyright holder for this preprint (which was not certified by peer review) is the author/funder. All rights reserved. No reuse allowed without permission.

and control cells into retinal cells, immunocytochemical analyses were performed on cells at the end of the differentiation period (day 30), to determine whether the cells expressed retinal cell markers. The cells were stained for either the disease-causing protein ATXN7, or the retinal cell markers CRX and RCVRN (**Figure 5b**). No obvious differences in morphology were observed between SCA7 patient and control-derived cells. The differentiated cells displayed varying expression levels of the retinal genes *CRX, PAX6, RCVRN* and *OTX2* (**Figure 5a** and **c**).

CAG repeat length

In order to confirm the size of the *ATXN7* CAG repeat alleles in mRNA from patient- and control-derived fibroblasts, iPSCs, NPCs and retinal cells, an RT-PCR-based assay was performed. The results were visualised on an agarose gel (**Figure S-1.2a** and **b**), and confirmed by automated fluorescent genotyping (data not shown). The length of the CAG repeat did not appear to fluctuate during reprogramming or differentiation, corresponding to previous reports in similar cell lines (Camnasio et al., 2012, Koch et al., 2011). This assay also confirmed that both the mutant and wild-type *ATXN7* alleles were expressed by all cell types, and that there were no obvious differences in allele expression in affected or unaffected cells.

Transcriptional dysregulation

To determine whether any transcriptional differences could be detected between SCA7 patient- and unaffected control-derived cell types, a panel of candidate genes was selected, which had previously been shown to be dysregulated in the retinal and cerebellar tissue of SCA7 mouse models and patient lymphoblasts (Yoo et al., 2003, Tsai et al., 2005, Abou-Sleymane et al., 2006, Chou et al., 2010). The panel included the following genes: *ATXN7*, brain expressed, X-linked 1 (*BEX1*), DnaJ (Hsp40) homolog, subfamily A, member 1 (*DNAJA1*), glutamate receptor, ionotropic, AMPA 2 (*GRIA2*), heat shock protein 27 (*HSP27*), heat shock protein 70 (*HSP70*), heat shock protein 105 (*HSP105*), oligodendrocyte transcription factor 1 (*OLIG1*), Phospholipase C, Beta 3 (*PLCB3*) and ubiquitin carboxyl-terminal esterase L1 (*UCHL1*). The expression of these genes was determined in fibroblasts, iPSCs, NPCs and retinal cells by means of qPCR. The expression of an additional panel of retinal genes was evaluated in the iPSC-derived retinal cells, including arrestin 3 (*ARR3*), cone-rod homeobox (*CRX*), guanine nucleotide binding protein (G protein), alpha transducing activity polypeptide 1 (*GNAT1*), Microphthalmia-associated transcription factor (*MITF*), neural retina leucine zipper (*NRL*), orthodenticle homeobox 2 (*OTX2*), paired box 6 (*PAX6*), recoverin (*RCVRN*), rhodopsin (*RHO*) and retinal pigment epithelium-specific protein 65kDa (*RPE65*).

No consistent, significant alterations in gene expression were observed between SCA7 patient and control fibroblasts or undifferentiated iPSCs (**Figure S-1.3**), highlighting the need to investigate neurodegenerative phenotypes in disease-relevant differentiated cell types.

In contrast to the fibroblasts and undifferentiated iPSCs, several genes were found to be significantly differentially expressed between SCA7 patient iPSC-derived retinal cells and NPCs, when compared to the equivalent cell type derived from unaffected control lines. Two genes were consistently downregulated in both retinal cells and NPCs. These included the disease-causing gene *ATXN7* ($p = 0.018$, NPCs, $p = 0.04$, retinal photoreceptors); and the K (lysine) acetyltransferase 2A (*KAT2A*), encoding GCN5, the histone acetyltransferase (HAT) component of the STAGA transcription coactivator complex ($p = 0.003$, NPCs, $p = 0.02$, retinal photoreceptors) (**Figure 6**).

Six genes were differentially expressed in either SCA7 patient photoreceptors or NPCs, but not both. Those specific to SCA7 photoreceptors included *GRIA2*, encoding the glutamate receptor, ionotropic, AMPA2 (GluR2) (downregulated, $p = 0.04$); and three retinal-specific genes, *OTX2* (upregulated, $p = 0.002$), *RCVRN* (downregulated, $p = 0.01$) and *RPE65* (upregulated, $p = 0.001$), which were not

bioRxiv preprint doi: https://doi.org/10.1101/288480; this version posted March 25, 2018. The copyright holder for this preprint (which was not certified by peer review) is the author/funder. All rights reserved. No reuse allowed without permission.

assessed in NPCs. NPC-specific alterations in expression were identified in the heat shock protein genes *DNAJA1* ($p = 0.04$) and *HSP70* ($p = 0.04$), both of which were found to be downregulated in SCA7-patient derived cells.
Finally, *BEX1*, an interactor of the p75 neurotrophin receptor, which regulates neurotrophin signalling and neuronal differentiation, was found to be upregulated in SCA7 photoreceptors ($p=0.0006$), and downregulated in SCA7 NPCs ($p = 0.03$), indicative of a possible differential response by the different cell types to the presence of mutant ATXN7.
As expected, a considerable degree of intra- and inter-individual variability was observed, with some genes showing significant changes in gene expression in one SCA7 patient line, but not another. Given the small number of lines used, however, emphasis was placed on those genes showing robust alterations in expression across all patient lines assessed.

4. Discussion

This study describes the generation and characterisation of the first iPSCs from the South African SCA7 patient cohort, through the transduction of patient dermal fibroblasts with Sendai viral vectors (Nishimura et al., 2011, Nakanishi and Otsu, 2012), as well as the differentiation of these iPSCs into neurons and retinal photoreceptors. This is the first report to include multiple patients, and to demonstrate a phenotype in disease-relevant cell types. To our knowledge, it is only the second report of iPSCs generated from SCA7 patients (Luo et al., 2012).

The SCA7 patient iPSCs generated in this study were shown to be able to differentiate into a homogeneous population of NPCs, capable of self-renewal for up to 30 passages, and with morphological similarities to neuroepithelial cells, as has been previously reported (Li et al., 2011). The generation of sustainable populations of neural precursors from SCA7 patients is significant, as these cells may act as a starting point for the generation of numerous disease-affected neuronal subtypes, which can be expanded for large-scale experiments at relatively low cost.

Both patient- and control- derived NPCs appeared capable of differentiating into neurons expressing βIII-Tubulin and GABA, with comparable efficiencies. This corresponds with results from previous studies of neurodegenerative conditions, including other polyQ diseases (Soldner et al., 2009, Koch et al., 2011, Camnasio et al., 2012), which found no difference in differentiation potential between patient and control iPSCs. In addition, no obvious difference in the ability to generate GABA-positive processes could be detected between SCA7 and control iPSC-derived neurons.

Electrophysiological studies were carried out to establish whether there were any functional differences in the intrinsic properties of patient and control cells. The majority of cells recorded were capable of generating spiking activity including single and multiple action potentials, an indication of neuronal maturity (Moody and Bosma, 2005). Despite the presence of significant differences in spiking responses between the four cell lines, we did not observe a reliable trend between the control and patient derived neurons. This is consistent with our observations of voltage-gated sodium and potassium currents, which underlie spiking activity. Significant variability, perhaps due to unappreciated differences in culturing conditions between cell lines, may have masked our ability to detect a reliable difference in spiking responses due to mutant ATXN7. Alternatively, it may be that mutant ATXN7 does not affect the spiking properties of neurons at early stages of development, suggesting that an extrinsic stressor of some kind might be required to elicit a pathological phenotype. Indeed, similar functional analysis of neurons derived from patients with SCA3, a related polyQ-repeat disorder, showed no difference between control and patient cells until neurons were excited via bath application of glutamate (Koch et al., 2011).

bioRxiv preprint doi: https://doi.org/10.1101/288480; this version posted March 25, 2018. The copyright holder for this preprint (which was not certified by peer review) is the author/funder. All rights reserved. No reuse allowed without permission.

Importantly, we did observe differences in resting membrane potential and input resistance between control and SCA7 patient derived neurons. Patient cells had more negative resting membrane potentials and increased input resistance compared to control cells. Both of these differences would serve to reduce the excitability of neurons containing mutant ATXN7 in response to synaptic input. Reductions in Purkinje cell excitability have previously been observed in animal models of SCA1 and SCA2 (Duvick et al., 2010, Hansen et al., 2012) and could represent a common functional endpoint in several polyQ disorders (Choppra et al., 2014). Future work will involve exploring the underlying mechanisms which might explain these differences in resting membrane potential and input resistance. Importantly, it will be necessary to repeat this physiological functional analysis on iPSC derived neurons of the Purkinje cell lineage in order to fully recapitulate the cerebellar-specific elements of the disease using the recently published protocols (Muguruma, 2017, Watson et al., 2018).

Retinal differentiation of iPSCs yielded a heterogeneous cell population after 30 days, containing a large proportion of cells expressing the photoreceptor markers CRX and RCVRN, as well as retinal cell genes *PAX6*, *OTX2*, *CRX* and *NRL* in the differentiating cells. The cells expressed varying levels of the photoreceptor genes, *RCVRN* and *RHO*, confirming that the retinal differentiation protocol was capable of producing cells expressing markers of "mature" photoreceptors, albeit at relatively low levels of efficiency.

A PCR-based assay was used to confirm the size of the *ATXN7* CAG repeat alleles in cDNA from patient- and control-derived fibroblasts, iPSCs, neural and retinal cells. Besides serving as a "fingerprinting" assay, confirming the identity of the lines, these results offered a semi-quantitative analysis of the expression levels of mutant and wildtype *ATXN7* alleles, confirming that both alleles were expressed at approximately equal levels in all cell lines. Despite the inherent instability of the CAG repeat within the *ATXN7* gene (Monckton et al., 1999), automated fluorescent genotyping of the PCR products indicated that no contractions or large-scale expansions had occurred during either reprogramming or differentiation, consistent with previous reports of other iPSC-derived models of polyQ disorders, including SCA3 and HD (Koch et al., 2011, Camnasio et al., 2012).

Immunocytochemical analysis of ATXN7 expression in SCA7 patient neural and retinal cells showed diffuse expression within the nucleus (neurons) or nucleus and cytoplasm (retinal photoreceptors). No obvious intranuclear inclusions were observed in either the iPSCs or the differentiated cells. This strongly suggests that the differentiated cells represent a population of cells at an early stage of development, rather than recapitulating the age or disease stage of the patient from which the primary cells were derived. Previous studies employing similar models for the study of neurodegenerative disease have raised concerns regarding the relevance of modelling adolescent- and adult-onset diseases over the short lifespan of cultured neurons, suggesting that pathological hallmarks of disease such as the formation of aggregates may take decades to manifest, requiring the gradual accumulation of toxic proteins as a result of age-dependent deficiencies in protein homeostasis (Soldner et al., 2009, Hartl et al., 2011). Although some studies suggest that aggregates may be detected at earlier stages, the major determinants of aggregate formation remain the length of the polyQ expansion, and the levels of expression of the polyQ-containing protein (Miller et al., 2010, Arrasate et al., 2004). Thus, a cell line derived from an individual expressing endogenous levels of a moderately expanded ATXN7 protein may be less likely to demonstrate an observable cellular phenotype. Alternatively, the aggregation of mutant protein may require prolonged periods in culture, or an exogenous trigger, such as exposure to oxidative stress or neurotoxins, or excitation-induced calcium influx (Koch et al., 2011).

The role of transcriptional dysregulation in the polyQ diseases has been extensively documented, particularly in cell and animal models of SCA7 (Abou-Sleymane et al., 2006, Chou et al., 2010, Yoo

bioRxiv preprint doi: https://doi.org/10.1101/288480; this version posted March 25, 2018. The copyright holder for this preprint (which was not certified by peer review) is the author/funder. All rights reserved. No reuse allowed without permission.

et al., 2003, Tsai et al., 2005, Zijlstra et al., 2010, La Spada et al., 2001). The identification of gene expression changes, which precede the onset of symptoms, suggests strongly that alterations in transcription may be among the earliest manifestations of disease (Helmlinger et al., 2006b). Thus, it follows that gene expression changes may be used as a tool to identify a disease-associated phenotype in cells representing early stages of development (Feyeux et al., 2012).

In order to investigate gene expression changes in the SCA7 iPSCs and iPSC-derived neurons generated here, a panel of candidate transcripts were selected, in which robust changes had been previously demonstrated (Palhan et al., 2005, Chou et al., 2010, Tsai et al., 2005, Sopher et al., 2011, Wang et al., 2010, Luthi-Carter et al., 2002). iPSC-derived neurons and retinal photoreceptors displayed changes in expression of these key transcripts, suggesting that these cells may serve as useful models of neurodegenerative disease progression and for the testing of potential therapies (**Figure 6**).

Of the three genes consistently downregulated across both differentiated cell types, two (*ATXN7* and *KAT2A*) encode components of the STAGA transcriptional co-activator complex. Previous studies in SCA7 patient fibroblasts and mouse models have demonstrated a disease-associated increase in *ATXN7* expression, mediated by non-coding RNAs (Tan et al., 2014, Sopher et al., 2011). The contradictory decrease in *ATXN7* expression in SCA7 NPCs and photoreceptors observed here could reflect the early developmental stage of the cells, but further analysis of the regulatory pathways will be required in order to elucidate the basis for this apparent decrease in the disease-causing protein in affected cell types. *KAT2A* encodes the histone acetyltransferase GCN5. Although there are no established links between *ATXN7* and the expression of *KAT2A*, numerous studies have identified a functional interaction between the two proteins, which results in changes in STAGA activity in *in vitro* and *in vivo* models of SCA7 (Palhan et al., 2005, Helmlinger et al., 2006a, Chen et al., 2011, Lan et al., 2015, Paulsen et al., 2017). Loss of GCN5 expression has been shown to result in increased retinal degeneration in SCA7 mice (Chen et al., 2011).

The interaction between ATXN7 and CRX has been hypothesised to be a key factor behind the development of retinal degeneration in SCA7 patients (La Spada et al., 2001). Therefore the expression of multiple known CRX targets, which were previously shown to be down-regulated in SCA7 mice, were included in the gene expression experiments. None of these target genes (including *ARR3*, *GNAT1* or *RHO*) showed consistent changes in patient cells. However, transcriptional changes in the expression of additional retinal genes, including *OTX2* (involved in the determination of photoreceptor cell fate), *RCVRN* (expressed in photoreceptors), and *RPE65* (expressed in retinal pigment epithelial cells), were noted in the patient derived cells. A significant degree of heterogeneity was observed in the differentiated retinal cells, both in terms of morphology, and gene/protein expression (**Figure 5**), therefore additional investigation will be required to determine whether these differences can be attributed to experimental differences or pathogenic mechanisms.

Downregulation of the HSP genes *HSP70* and *DNAJA1* was observed in SCA7 patient NPCs. A decrease in levels of these two HSPs has been previously reported in both SCA7 mice, and human patient lymphoblasts (Chou et al., 2010, Tsai et al., 2005). Although this decrease in expression was hypothesised in mice to represent an advanced stage of disease progression, the early developmental stage recapitulated by our model suggests that decreases in certain HSP genes may instead be an inherent defect, which could predispose certain populations of cells to degeneration.

The generation of patient-specific, disease-relevant cell types is particularly important in neurodegenerative diseases; as such cells provide a unique model in which to evaluate disease pathogenesis without the complications associated with transgene overexpression in cell or animal

bioRxiv preprint doi: https://doi.org/10.1101/288480; this version posted March 25, 2018. The copyright holder for this preprint (which was not certified by peer review) is the author/funder. All rights reserved. No reuse allowed without permission.

models. In addition, the use of cells containing the patient's own genetic background offers the opportunity to investigate potential modifiers of disease onset and progression (Marsh and Thompson, 2006; Bilen and Bonini, 2007,). Perhaps most importantly to the South African context, iPSC-derived neurons provide the first opportunity to evaluate the efficacy of the allele-specific RNAi-based therapy developed by Scholefield et al. (2009), in disease-affected cells.

One significant caveat of this study remains the small number of patients assessed – a consequence of the rare nature of the condition, and the challenges associated with patient recruitment in a developing world setting, in which many of those affected are unable to access tertiary healthcare. Future studies will focus on recruitment, in order to extend these investigations in a larger patient cohort. To control for the inherent genetic variability associated with comparisons between unrelated patients, future work will also focus on the generation of isogenic control lines, by means of CRISPR/Cas9-mediated genome editing.

Nevertheless, the SCA7 iPSCs generated here serve as a resource for differentiation into a variety of disease-associated cell types, providing an ideal model in which to study neurodegenerative diseases. The results of this study provide the first evidence of a disease phenotype in iPSC-derived cells from the South African SCA7 patient cohort, paving the way for future analysis of pathogenesis, and the development of population-specific therapies.

5. Abbreviations

CRX, cone-rod homebox; iPSC, induced pluripotent stem cells; NPC, neuronal progenitor cells; PCR, polymerase chain reaction; polyQ, polyglutamine; SCA7, spinocerebellar ataxia type 7; SeVdp, Sendai virus vectors; STAGA; SPT3-TAF9-ADA-GCN5 acetyltransferase.

6. Supporting Information

Figure S-1.1 shows a representative karyogram of an iPSC line, showing no gross structural abnormalities. **Figure S-1.2** shows how iPSCs, retinal cells and NPCs were differentiated by semi-quantitative PCR. **Figure S-1.3** shows transcriptional changes in SCA7 patient-derived fibroblasts, compared to unaffected control fibroblasts.
Summary of SCA7 patient and unaffected control cell lines, genotypes and ages is shown in **Table S-1.1.** The various antibodies for immunocytochemistry used are summarised in **Table S-1.2** while the primer sequences used are shown in **Table S-1.3**.

7. Conflict of Interests

The authors declare that the research was conducted in the absence of any commercial or financial relationships that could be construed as a potential conflict of interest.

8. Author Contributions

LMW, iPSC culture experimental work for neuronal cells, molecular studies, imaging, writing of manuscript; **DCS**, iPSC culture experimental work for retinal cells, imaging, molecular studies, writing of manuscript; **JVR**, electrophysiology experimental work, data analysis thereof, writing of manuscript; **RJB**, electrophysiology experimental work, data analysis thereof, writing of manuscript; **RB**, iPSC generation; **JS**, technical supervision for iPCS culture and imaging; **SAC**, supervision of iPSC culture and molecular experiments; **MJAW**, supervision of molecular studies; **SHK**, supervision

bioRxiv preprint doi: https://doi.org/10.1101/288480; this version posted March 25, 2018. The copyright holder for this preprint (which was not certified by peer review) is the author/funder. All rights reserved. No reuse allowed without permission.

of iPSC differentiation, assisted in writing of manuscript; **LJG**, principle investigator, patient recruitment, supervision of iPSC culture and molecular studies and assisted in writing of manuscript.

9. Funding

Funding for this work was provided by Ataxia UK, Commonwealth Scholarship Commission (UK), John Fell OUP Fund, National Research Foundation (South Africa), National Research Foundation (South Africa, Competitive Programme for Rated Researchers CPR20110624000019696), Medical Research Council (South Africa), Harry Crossley Foundation, Deutscher Akademischer Austausch Dienst, University of Cape Town Research Council, Wellcome Trust, Parkinson's Disease UK, Medical Research Council UK, Blue Brain Project, and the James Martin 21st Century School. Electrophysiology equipment was provided by the École Polytechnique Fédérale de Lausanne, Switzerland.

10. Acknowledgements

The authors thank Dr Mahito Nakanishi for kind provision of the Sendai virus vector, Ms Jane Vowles for assistance with iPSC generation, and Ms Theresa Ruppelt and colleagues at the South African National Health Laboratory Service for karyotype analyses. We honour the late Ms Ingrid Baumgarten for her invaluable assistance over many years, particularly in establishing patient fibroblast cultures.

11. References

Abou-Sleymane G, Chalmel F, Helminger D, Lardenois A, Thibault C, Weber C, et al. Polyglutamine expansion causes neurodegeneration by altering the neuronal differentiation program. Human Molecular Genetics (2006) 15: 691-703. doi: 10.1093/hmg/ddi483s.

Ansorge O, Giunti P, Michalik A, Van Broeckhoven C, Harding B, Wood N, et al. Ataxin-7 aggregation and ubiquitination in infantile SCA7 with 180 CAG repeats. Annals of Neurology (2004) 56**:** 448-452. doi: 10.1002/ana.20230.

Arrasate M, Mitra S., Schweitzer ES, Segal MR & Finkbeiner S Inclusion body formation reduces levels of mutant huntingtin and the risk of neuronal death. Nature (2004) 431**:** 805-810. doi: 10.1038/nature02998.

Belinsky GS, Moore AR, Short SM, Rich MT & Antic SD. Physiological properties of neurons derived from human embryonic stem cells using a dibutyryl cyclic AMP-based protocol. Stem Cells Development (2011) 20:1733-1746. doi: 10.1089/scd.2010.0501.

Belinsky GS, Rich MT, Sirois CL, Short SM, Pedrose E, Lachman HM & Antic SD. Patch-clamp recordings and calcium imaging followed by single-cell PCR reveal the developmental profile of 13 genes in iPSC-derived human neurons. Stem Cell Research (2014) 12**:** 101-118. doi: 10.1089/scd.2010.0501.

Boucherie C, Mukherjee S, Henckaerts E, Thrasher AJ, Sowden JC and Ali RR. Brief report: Self-organizing neuroepithelium from human pluripotent stem cells facilitates derivation of photoreceptors. Stem cells (2013) 31:408-414. doi: 10.1002/stem.1268.

Bilen J & Bonini NM. Genome-wide screen for modifiers of ataxin-3 neurodegeneration in Drosophila. PLoS Genetics (2007) 3**:** e177. doi: 10.1371/journal.pgen.0030177.

Bustin SA, Benes V, Garson JA, Hellemans J, Huggett J, Kubista M, et al. The MIQE guidelines: minimum information for publication of quantitative real-time PCR experiments. Clinical chemistry (2009) 55: 611-622. doi: 10.1111/eci.12801

bioRxiv preprint doi: https://doi.org/10.1101/288480; this version posted March 25, 2018. The copyright holder for this preprint (which was not certified by peer review) is the author/funder. All rights reserved. No reuse allowed without permission.

552 Camnasio S, Carri AD, Lombardo A, Grad I, Mariotti C, Ca stucci A, Rozell B, Riso PL, Castiglioni
553 V & Zuccato C. The first reported generation of several induced pluripotent stem cell lines from
554 homozygous and heterozygous Huntington's disease patients demonstrates mutation related enhanced
555 lysosomal activity. Neurobiology of Disease (2012) 46**:** 41-51. doi: 10.1016/j.nbd.2011.12.042.

556 Chen TC, Gatchel JR, Lewis RW, Mao CA, Grant PA, Zoghbi HY, et al. Gcn5 loss-of-function
557 accelerates cerebellar and retinal degeneration in a SCA7 mouse model. Human Molecular Genetics
558 (2011) 21: 394-405. doi: 10.1093/hmg/ddr474.

559 Chou AH, Chen CY, Chen SY, Chen Wj, Chen YL, Weng YS, et al. Polyglutamine-expanded ataxin-
560 7 causes cerebellar dysfunction by inducing transcriptional dysregulation. Neurochemistry
561 International (2010) 56**:** 329-339. doi: 10.1016/j.neuint.2009.11.003.

562 Duvick L, Barnes J, Ebner B, Agrawal S, Andresen M, Lim J, et al. SCA1-like disease in mice
563 expressing wild-type ataxin-1 with a serine to aspartic acid replacement at residue 776. Neuron (2010)
564 67 929-935. doi: 10.1016/j.neuron.2010.08.022.

565 Einum DD, Townsend JJ, Ptacek LJ & FU YH. Ataxin-7 expression analysis in controls and
566 spinocerebellar ataxia type 7 patients. Neurogenetics (2001) 3**:** 83-90.

567 Feyeux M, Bougois-Rocha F, Redfern A, Giles P, LeFort N, Aubert S, et al. Early transcriptional
568 changes linked to naturally occurring Huntington's disease mutations in neural derivatives of human
569 embryonic stem cells. Human Molecular Genetics (2012) 21**:** 3883-3895. doi: 10.1093/hmg/dds216.

570 Frechney RI. Specialized cells. Culture of Animal Cells: A Manual of Basic Technique and Specialized
571 Applications. New Jersey: Wiley-Blackwell (2000). 383-432.

572 Garden GA & La Spada. Molecular pathogenesis and cellular pathology of spinocerebellar ataxia type
573 7 neurodegeneration. The Cerebellum (2008) 7**:** 138-149.

574 Garden GA, Libby RT, Fu YH, Kinoshita Y, Huang J, Possin DE et al. Polyglutamine-expanded ataxin-
575 7 promotes non-cell-autonomous purkinje cell degeneration and displays proteolytic cleavage in ataxic
576 transgenic mice. Journal of Neuroscience (2012) 22**:** 4897-4905.

577 Gouw L, Digre K, Harris C, Haines J & Ptacek :OUW, L., DIGRE, K., HARRIS, C., HAINES, J. &
578 PTACEK, L. Autosomal dominant cerebellar ataxia with retinal degeneration Clinical,
579 neuropathologic, and genetic analysis of a large kindred. Neurology, (1994) 44**:** 1441-1441. doi:
580 10.1111/j.1399-0004.2006.00680.

581 Greenberg J, Solomon G, Vorster A, Heckmann J & Bryer A. Origin of the SCA7 gene mutation in
582 South Africa: implications for molecular diagnostics. Clinical genetics (2006) 70**:** 415-417. doi:
583 10.1111/j.1399-0004.2006.00680.

584 Handsen ST, Meera P, Otis TS & Pulst SM. Changes in Purkinje cell firing and gene expression
585 precede behavioral pathology in a mouse model of SCA2. Human Molecular Genetics (2012) 22**:** 271-
586 283. doi:10.1093/hmg/dds427.

587 Hartl FU, Bracher A & Hayer-Hartl M. Molecular chaperones in protein folding and proteostasis.
588 Nature (2011) 475**:** 324. doi: 10.1038/nature10317.

589 Helminger D, Hardy S, Eberlin A, Devys D & Tora L. Both normal and polyglutamine-expanded
590 ataxin-7 are components of TFTC-type GCN5 histone acetyltransferase-containing complexes.
591 Biochemical Society Symposia, 2006a. London; Portland on behalf of The Biochemical Society;
592 (1999) 155.

593 Helminger D, Tora L & Devys D. Transcriptional alterations and chromatin remodeling in
594 polyglutamine diseases. Trends in Genetics (2006) 22**:** 562-570.

bioRxiv preprint doi: https://doi.org/10.1101/288480; this version posted March 25, 2018. The copyright holder for this preprint (which was not certified by peer review) is the author/funder. All rights reserved. No reuse allowed without permission.

595 Jonasson J, Strom AL, Hart P, Brannstrom T, Forsgren L & Holmberg M. Expression of ataxin-7 in
596 CNS and non-CNS tissue of normal and SCA7 individuals. Acta Neuropathologica (2002) 104**:** 29-37.
597 doi: 10.1007/s00401-001-0514-4.

598 Koch P, Breuer P, Peitz M, Jungverdorben J, Kesavan J, Poppe D, et al. Excitation-induced ataxin-3
599 aggregation in neurons from patients with Machado–Joseph disease. Nature (2011) 480**:** 543. doi:
600 10.1038/nature10671.

601 Larionov A, Krause A and Miller W. A standard curve based method for relative real time PCR data
602 processing. BMC bioinformatics (2005) 6: 62-77. 10.1186/1471-2105-6-62

603 La Spada AR, Fu YH, Sopher BL, Libby RT, Wang X, Li LY, et al. Polyglutamine-expanded ataxin-
604 7 antagonizes CRX function and induces cone-rod dystrophy in a mouse model of SCA7. Neuron
605 (2001) 31: 913-927.

606 Li W, Sun W, Zhang Y, Wei W, Ambasudhan R, Xia P, Talantova M, et al. Rapid induction and long-
607 term self-renewal of primitive neural precursors from human embryonic stem cells by small molecule
608 inhibitors. Proceedings of the National Academy of Sciences (2011) 108**:** 8299-8304.

609 Luo Y, Fan Y, Zhou B, Xu Z, Chen Y & Sun X. Generation of induced pluripotent stem cells from
610 skin fibroblasts of a patient with olivopontocerebellar atrophy. The Tohoku Journal of Experimental
611 Medicine (2012) 226**:** 151-159.

612 Luthi-Carter R, Strand AD, Hanson SA, Kooperberg C, Schilling G, La Spada AR, et al. Polyglutamine
613 and transcription: gene expression changes shared by DRPLA and Huntington's disease mouse models
614 reveal context-independent effects. Human Molecular Genetics (2002) 11**,** 1927-1937.

615 March JL & Thompson LM. Drosophila in the study of neurodegenerative disease. Neuron (2006) 52**:**
616 169-178. doi: 10.1016/j.neuron.2006.09.025.

617 Martl M, Mulero L, Pardo C, Morera C, Carrio M, Laricchia-Robbio, et al. Characterization of
618 pluripotent stem cells. Nature Protocols (2013) 8**:** 223. doi: 10.1038/nprot.2012.154.

619 Miller J, Arrasate M, Shaby BA, Mitra S, Masliah E & Finkbeiner S. Quantitative relationships
620 between huntingtin levels, polyglutamine length, inclusion body formation, and neuronal death provide
621 novel insight into huntington's disease molecular pathogenesis. Journal of Neuroscience (2010) 30**:**
622 10541-10550. doi: 10.1523/JNEUROSCI.0146-10.2010.

623 Monckton DG, Cayuela ML, Gould FK, Brock GJ, de Silva R & Ashizawa T. Very large (CAG) n
624 DNA repeat expansions in the sperm of two spinocerebellar ataxia type 7 males. Human Molecular
625 Genetics (1999) 8**:** 2473-2478.

626 Moody & Bosma MM. Ion channel development, spontaneous activity, and activity-dependent
627 development in nerve and muscle cells. Physiological Reviews (2005) 85**:** 883-941. doi:
628 10.1152/physrev.00017.2004.

629 Moore AR, Filipovic R, Mo Z, Rasband MN, Zecevic N & Antic SD. Electrical excitability of early
630 neurons in the human cerebral cortex during the second trimester of gestation. Cerebral Cortex (2009)
631 19:1795-1805. doi: 10.1093/cercor/bhn206.

632 Muguruma, K. Self-Organized Cerebellar Tissue from human pluripotent stem cells and disease
633 modeling with patient-derived iPSCs. The Cerebellum (2017) 1597: 1-5. doi: 10.1007/978-1-4939-
634 6949-4_3.

635 Nakanishi M & Otsu M. Development of Sendai virus vectors and their potential applications in gene
636 therapy and regenerative medicine. Current Gene Therapy (2012) 12**:** 410-416.

bioRxiv preprint doi: https://doi.org/10.1101/288480; this version posted March 25, 2018. The copyright holder for this preprint (which was not certified by peer review) is the author/funder. All rights reserved. No reuse allowed without permission.

637 Nishimura K, Sano M, Phtaka M, Furuta B, Imemura Y, Nakajima Y, et al. Development of defective
638 and persistent Sendai virus vector a unique gene delivery/expression system ideal for cell
639 reprogramming. Journal of Biological Chemistry (2011) 286**:** 4760-4771. doi:
640 10.1074/jbc.M110.183780.

641 Orr HT & Zoghbi HY Trinucleotide repeat disorders. Annuals Reviews Neuroscience (2007) 30**:** 575-
642 621. doi: 10.1146/annurev.neuro.29.051605.113042.

643 Palhan VB, Chen S, Peng GH, Tjernberg A, Gamper AM, Fan Y, et al. Polyglutamine-expanded ataxin-
644 7 inhibits STAGA histone acetyltransferase activity to produce retinal degeneration. Proceedings of
645 the National Academy of Sciences of the United States of America (2005) 102: 8472-8477. doi:
646 10.1073/pnas.0503505102.

647 Paulson HL, Shakkottai VG, Clark HB and Orr HT. Polyglutamine spinocerebellar ataxias—from
648 genes to potential treatments. Nature Reviews Neuroscience (2017) 18: 613 - 626. doi:
649 10.1038/nrn.2017.92.

650 Perrier AL, Tabar V, Barberi T, Rubio ME, Bruses J, Topf N, et al. Derivation of midbrain dopamine
651 neurons from human embryonic stem cells. Proceedings National Academy Science U S A (2004)
652 101:12543-12548. doi: 10.1073/pnas.0404700101.

653 Scholefield J, Greenberg LJ, Weinberg MS, Arbuthnot PB, Abdelgany A & Wood MJ. Design of RNAi
654 hairpins for mutation-specific silencing of ataxin-7 and correction of a SCA7 phenotype. PloS One
655 (2009) 4: e7232. doi: 10.1371/journal.pone.0007232.

656 Scholefield J, Watson L, Smith D, Greenberg J & Wood MJ. Allele-specific silencing of mutant
657 Ataxin-7 in SCA7 patient-derived fibroblasts. European Journal of Human Genetics (2014) 22**:** 1369.
658 doi: 10.1038/ejhg.2014.39.

659 Smith D, Bryer A, Watson L & Greenberg LJ. Inherited polyglutamine spinocerebellar ataxias in South
660 Africa. South African Medical Journal (2012) 102**:** 683-686. doi: 10.1016/j.jns.2015.04.053.

661 Smith DC, Atadzhanov M, Mwaba M & Greenberg LJ. Evidence for a common founder effect amongst
662 South African and Zambian individuals with Spinocerebellar ataxia type 7. Journal of the Neurological
663 Sciences (2015) 354**:** 75-78. doi: 10.1016/j.jns.2015.04.053.

664 Soldner F, Hockemeyer D, Beard C, Gao Q, Bell GW, Cook EG, et al. Parkinson's disease patient-
665 derived induced pluripotent stem cells free of viral reprogramming factors. Cell (2009) 136**:** 964-977.
666 doi: 10.1016/j.cell.2009.02.013.

667 Sopher BL, Ladd, PD, Pineda VV, Libby RT, Sunkin SM, Hurley JB, et al. CTCF regulates ataxin-7
668 expression through promotion of a convergently transcribed, antisense noncoding RNA. Neuron (2007)
669 70**:** 1071-1084. doi: 10.1016/j.neuron.2011.05.027.

670 Strom AL, Forsgren L & Homberg M. A role for both wild-type and expanded ataxin-7 in
671 transcriptional regulation. Neurobiology of Disease (2005) 20**:** 646-655. doi:
672 10.1016/j.nbd.2005.04.018.

673 Takahashi K, Tanabe K, Ohnuke M, Narita M, Ichisaka T, Tomoda K & Yamanaka S. Induction of
674 pluripotent stem cells from adult human fibroblasts by defined factors. Cell (2007) 131**:** 861-872. doi:
675 10.1016/j.cell.2007.11.019.

676 Takahashi K, Yamanaka S. Induction of pluripotent stem cells from mouse embryonic and adult
677 fibroblast cultures by defined factors. Cell (2006) 126**:** 663-676. doi: 10.1016/j.cell.2006.07.024.

bioRxiv preprint doi: https://doi.org/10.1101/288480; this version posted March 25, 2018. The copyright holder for this preprint (which was not certified by peer review) is the author/funder. All rights reserved. No reuse allowed without permission.

678 Tan JY, Vance KW, Varela MA, Sirey T, Watson LM, Curtis HJ, et al. Cross-talking noncoding RNAs
679 contribute to cell-specific neurodegeneration in SCA7. Nature Structural and Molecular Biology
680 (2014) 21**:** 955. doi: 10.1038/nsmb0315-272b.

681 Taylor J, Grote SK, Xia J, Vandelft M, Graczyk J, Ellerby LM, et al. Ataxin-7 can export from the
682 nucleus via a conserved exportin-dependent signal. Journal of Biological Chemistry (2006) 281**:** 2730-
683 2739. doi: 10.1074/jbc.M506751200.

684 Todd TW & Lim J Aggregation formation in the polyglutamine diseases: protection at a cost?
685 Molecules and Cells (2013) 36**:** 185-194. doi: 10.1007/s10059-013-0167-x.

686 Tsai HF, Lin SJ, Li C & Hsieh M. Decreased expression of Hsp27 and Hsp70 in transformed
687 lymphoblastoid cells from patients with spinocerebellar ataxia type 7. Biochemical and biophysical
688 research communications (2005) 334**:** 1279-1286.

689 Wang HL, Chou AH, Lin AC, Chen SY, Weng YH & Yeh THANG, H.-L Polyglutamine-expanded
690 ataxin-7 upregulates Bax expression by activating p53 in cerebellar and inferior olivary neurons.
691 Experimental Neurology (2010) 224**:** 486-494. doi: 10.1016/j.expneurol.2010.05.011.

692 Watson LM, Wong MM & Becker EB. Induced pluripotent stem cell technology for modelling and
693 therapy of cerebellar ataxia. Open Biology (2015) 5: 150056. doi: 10.1098/rsob.150056.

694 Watson LM, Wong MM, Vowles J, Cowley SA and Becker EB. A Simplified Method for Generating
695 Purkinje Cells from Human-Induced Pluripotent Stem Cells. The Cerebellum (2018): 1-9. doi:
696 10.1007/s12311-017-0913-2.

697 Watson LM, Wood MJA, Smith DC, Scholefield J, Ballo R, Kidson S and Greenberg LJ.
698 Spinocerebellar ataxia type 7 in South Africa: epidemiology, pathogenesis and therapy: the new
699 millennium. *South African Medical Journal* (2016) *106*: 107-109. doi:
700 10.7196/SAMJ.2016.v106i6.11010.

701 Yoo SY, Pennesi ME, Weeber EJ, Xu B, Atkinson R, Chen S, et al. SCA7 knockin mice model human
702 SCA7 and reveal gradual accumulation of mutant ataxin-7 in neurons and abnormalities in short-term
703 plasticity. Neuron (2003) 37**:** 383-401.

704 Young JE, Gouw L, Propp S, Sopher BL, Taylor J, Lin A, et al. Proteolytic cleavage of ataxin-7 by
705 caspase-7 modulates cellular toxicity and transcriptional dysregulation. Journal of Biological
706 Chemistry (2007) 282**:** 30150-30160. doi: 10.1074/jbc.M705265200.

707 Zijlstra M, Rujano M, Van Waarde M, Vis E, Brunt E & Kampinga H. Levels of DNAJB family
708 members (HSP40) correlate with disease onset in patients with spinocerebellar ataxia type 3. European
709 Journal of Neuroscience (2010) 32**:** 760-770. doi: 10.1111/j.1460-9568.2010.07352.x.

710

711

712 **12. Figures**

bioRxiv preprint doi: https://doi.org/10.1101/288480; this version posted March 25, 2018. The copyright holder for this preprint (which was not certified by peer review) is the author/funder. All rights reserved. No reuse allowed without permission.

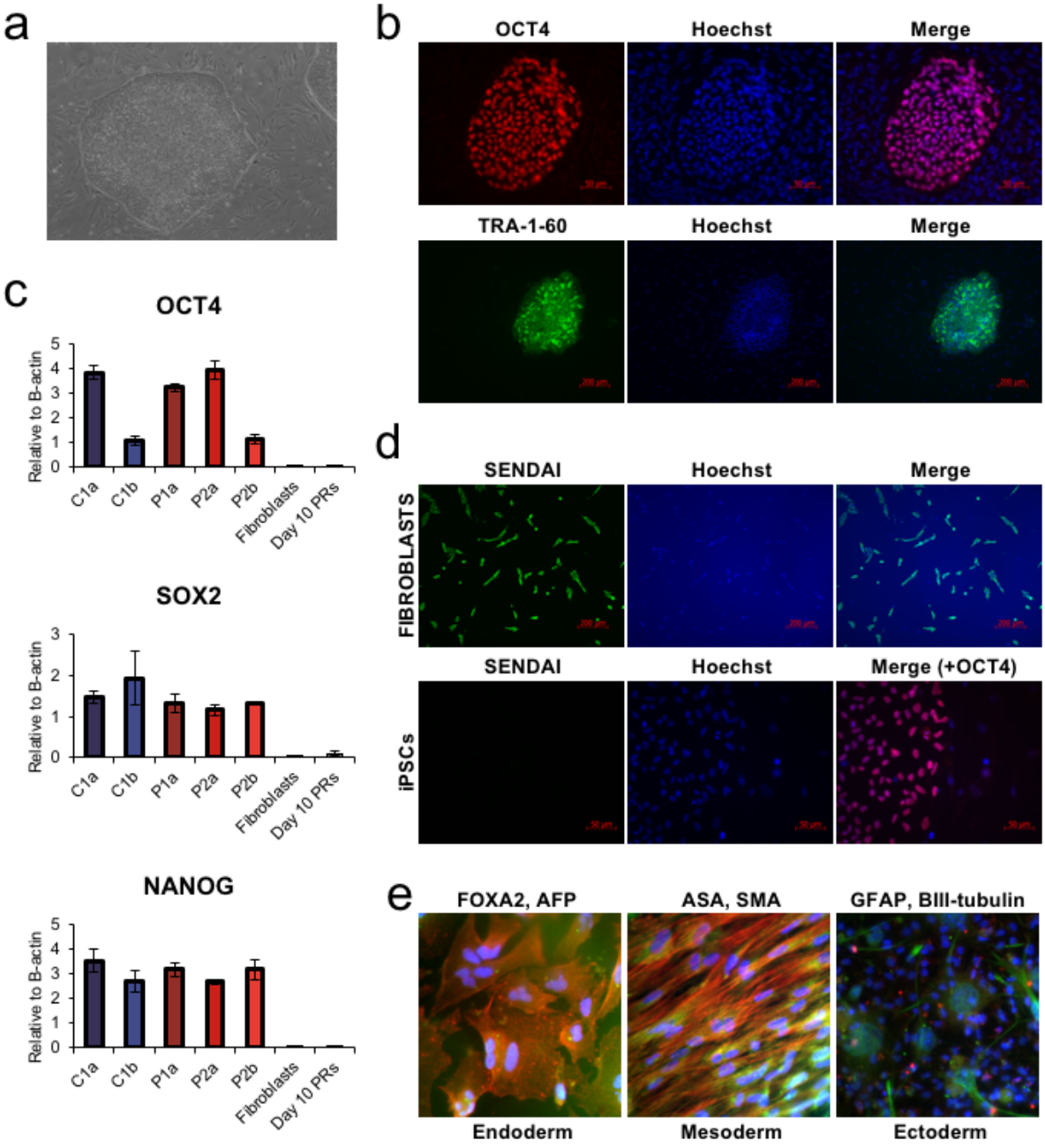

Figure1: iPSC characterisation. **a**) Morphology of iPSC colonies. Colonies could be seen as groups of tightly packed cells with a high nuclear-to-cytoplasm ratio. **b**) Representative immunocytochemistry image showing positive OCT4 staining (red, top panel) and TRA-1-60 staining (green, bottom panel) in iPSCs. **c**) Expression of pluripotency markers in iPSC lines, determined by qPCR. All five iPSC lines (P1a, P2a, P2b, C1a, C1b) expressed OCT4, SOX2 and NANOG, compared to low expression levels in the original donor fibroblasts, or cells subjected to the retinal differentiation protocol for 10 days (pooled data from lines P2b and C1b). All levels shown relative to beta actin (ACTB). d) Immunocytochemistry in newly infected fibroblasts (top panel) and iPSC colonies (bottom panel) co-stained with primary antibodies against OCT4 (red) and the viral nucleocapsid protein (green) showed effective silencing of the reprogramming Sendai virus. **e**) The five iPSC lines (P1a, P2a, P2b, C1a,

bioRxiv preprint doi: https://doi.org/10.1101/288480; this version posted March 25, 2018. The copyright holder for this preprint (which was not certified by peer review) is the author/funder. All rights reserved. No reuse allowed without permission.

C1b) were subjected to differentiation protocols to produce cells from either the endodermal, mesodermal or ectodermal lineages. Endodermal cells stained positive for either Forkhead box A2 (FOXA2, green) or Alpha-fetoprotein (AFP, red). Mesodermal cells expressed either Sarcomeric alpha actinin (ASA, green) or Smooth muscle actin (SMA, red). Ectodermal cells expressed Glial fibrillary acidic protein (GFAP, red) or βIII-tubulin (green).

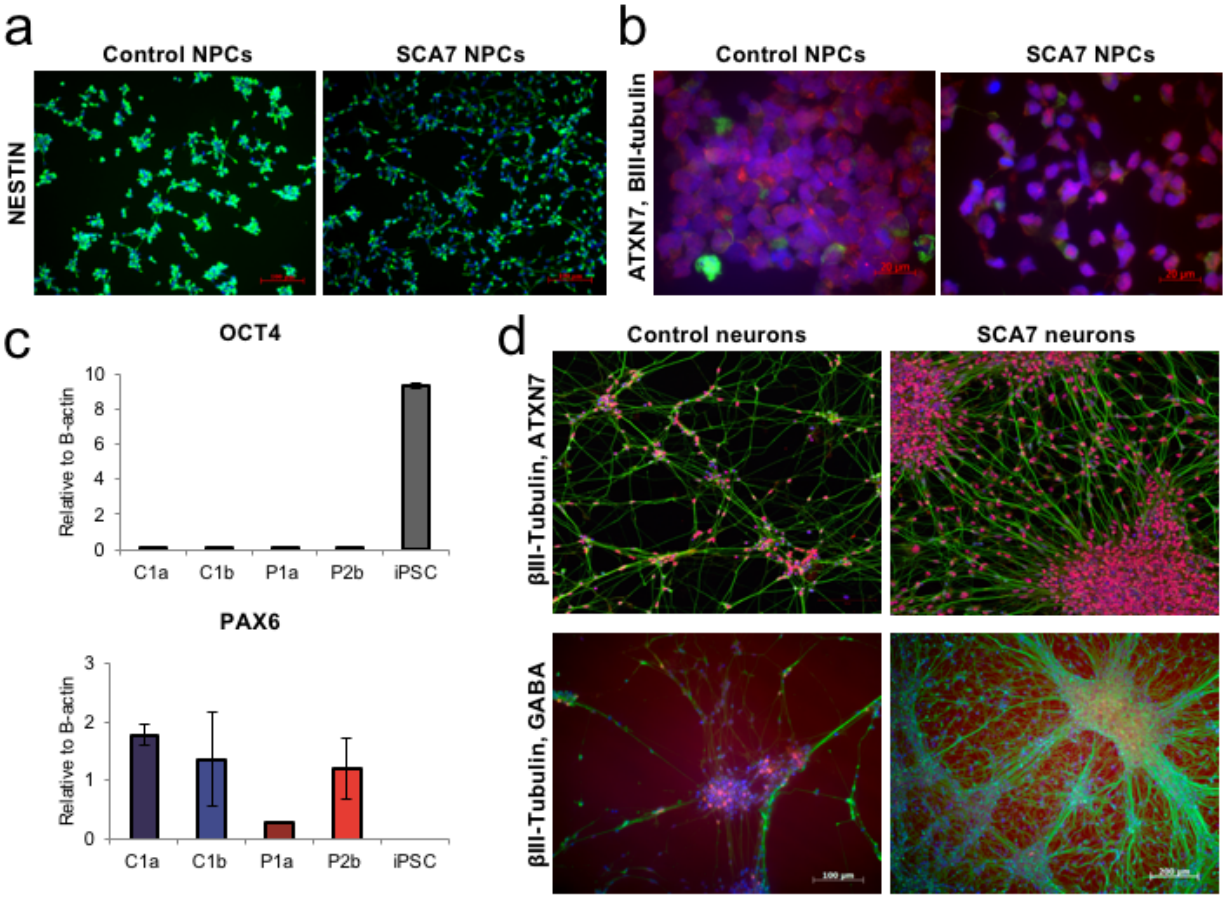

Figure 2: Characterisation of iPSC-derived NPCs. **a**) Representative images of control (left panel) and SCA7 patient (right panel) NPCs, expressing the early neural marker, Nestin (green). **b**) High magnification images showing nuclear expression of ATXN7 (red) in control (left) and patient (right) NPCs (Green: βIII-Tubulin). **c**) qPCR results indicating suppression of *OCT4* and upregulation of *PAX6* expression in NPCs, compared with the iPSC lines from which they were derived. All levels shown relative to beta actin (ACTB). **d**) Control (left) and SCA7 (right) NPC-derived neurons stain positive for βIII-Tubulin (green) and ATXN7 (red) after 14 days of differentiation (top panel). Both control (left) and SCA7 patient (right) NPCs produced a small proportion of GABA-positive neurons (red) after 14 days in culture (bottom panel) (Green: βIII-Tubulin).

bioRxiv preprint doi: https://doi.org/10.1101/288480; this version posted March 25, 2018. The copyright holder for this preprint (which was not certified by peer review) is the author/funder. All rights reserved. No reuse allowed without permission.

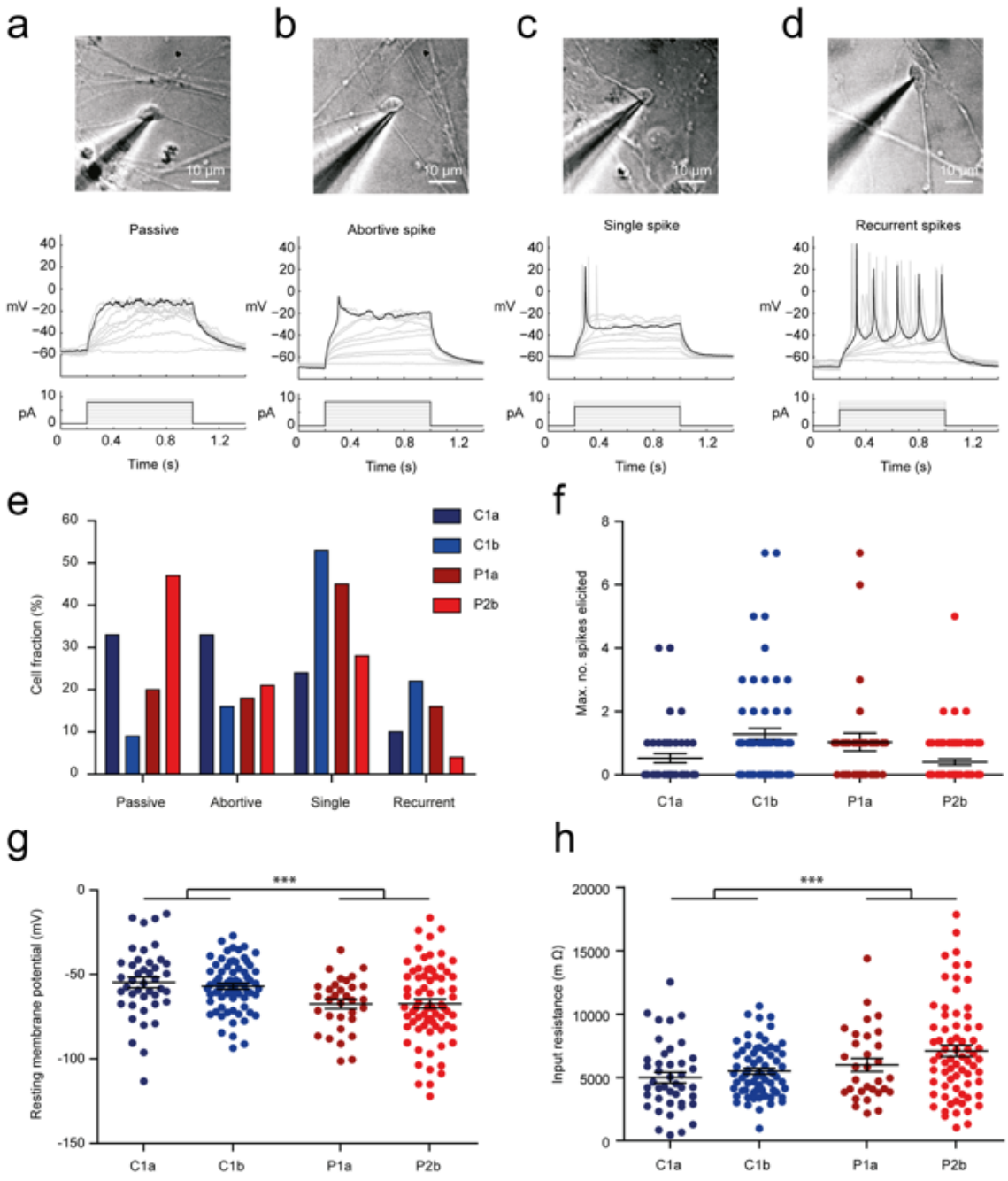

Figure 3: Patch-clamp analyses of iPSC derived neuronal cultures. Cells could be divided into four categories based on their spiking responses. a)-d) Differential interference contrast images of cells targeted for patch-clamp recordings (top). Whole-cell recordings in current clamp mode (middle) depict spiking patterns following injection of current (bottom). Cells fell into (**a**) 'passive', (**b**) 'abortive spike', (**c**) 'single spike' and (**d**) 'recurrent spikes' categories. **e**) The fraction of cells which fell into each category for cells derived from two control and two SCA7 patient iPSC lines. Note that although the cells derived from various iPSC lines exhibited different distributions of spiking responses, no trend between control and patient lines was observed. **f**) Maximum number of spikes elicited by current injection for each recorded cell according to the iPSC line. **g**) The resting membrane potentials of cells derived from SCA7 patients were significantly more negative than controls. **h**) Cell

bioRxiv preprint doi: https://doi.org/10.1101/288480; this version posted March 25, 2018. The copyright holder for this preprint (which was not certified by peer review) is the author/funder. All rights reserved. No reuse allowed without permission.

input resistance was also significantly increased in SCA7 patient lines as compared to control lines. Error bars denote mean +/- SEM, *** $p < 0.001$.

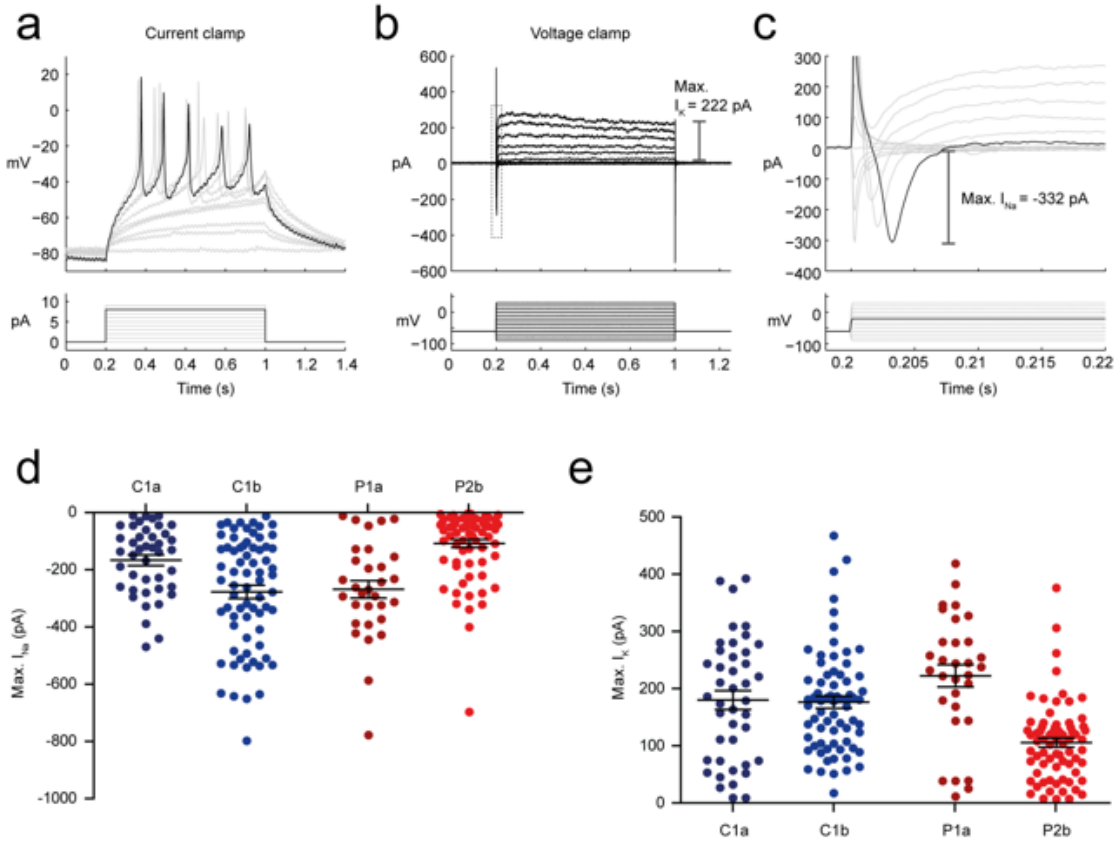

Figure 4: Sodium and potassium currents in neurons differentiated from control and patient iPS cell lines. **a**) Current-clamp recording demonstrating recurrent spikes elicited from a cell following current injection. **b**) Voltage-clamp recording from the same cell in 'a'. Membrane currents (top) were recorded following 10 mV voltage steps between -90 and 30 mV (bottom). Dashed gray rectangle indicates the position of voltage-gated sodium currents (enhanced in '**c**'). Maximum potassium current is indicated 'right'. **c**) Zoom-in of rectangle in 'b' with the maximum sodium current highlighted. Population data from the four iPSC lines for maximum voltage-gated sodium (**d**) and maximum potassium (**e**) currents respectively. No consistent trend between control and patient lines was observed. Error bars denote mean +/- SEM.

bioRxiv preprint doi: https://doi.org/10.1101/288480; this version posted March 25, 2018. The copyright holder for this preprint (which was not certified by peer review) is the author/funder. All rights reserved. No reuse allowed without permission.

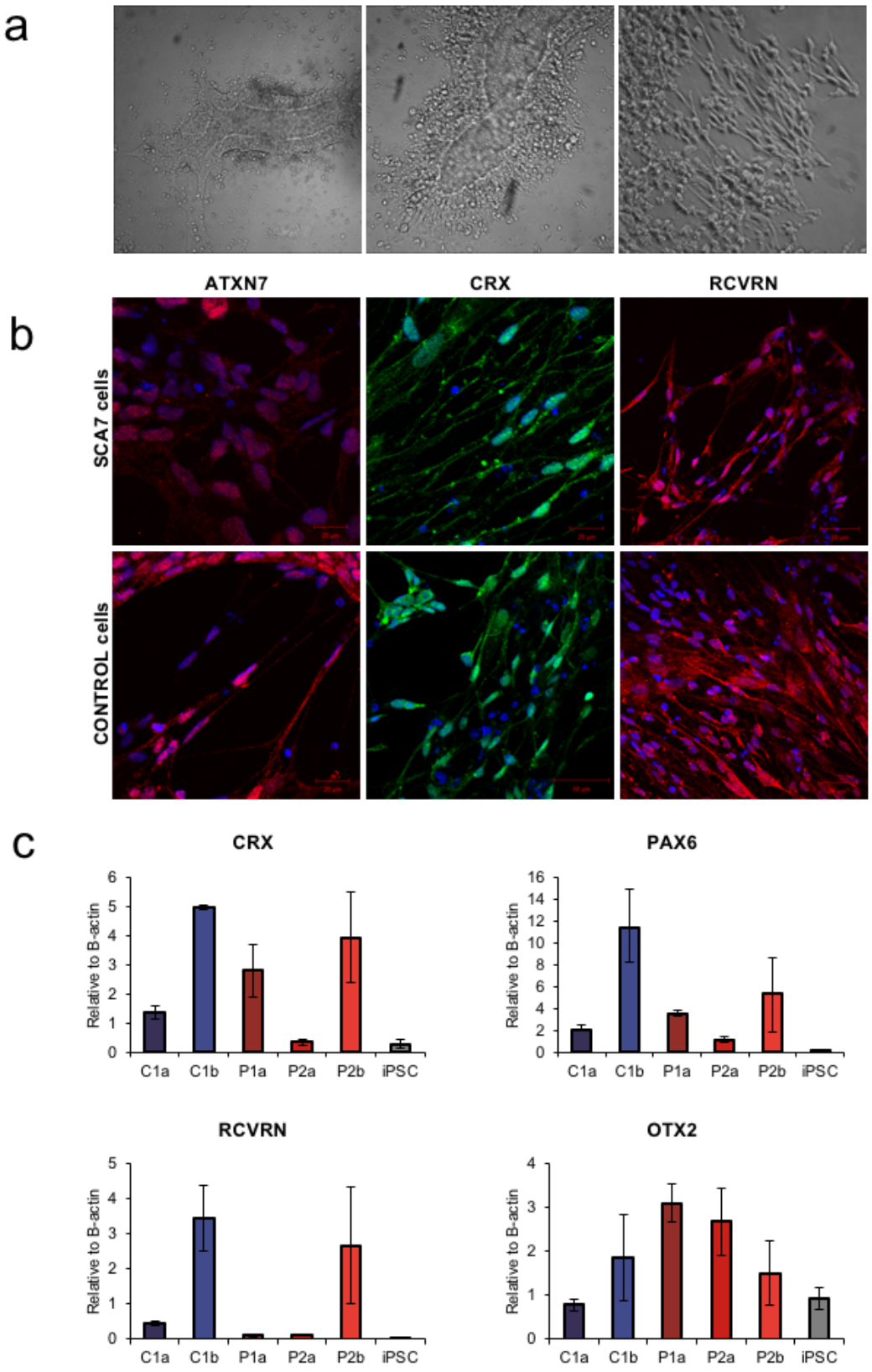

Figure 5: Characterisation of iPSC-derived retinal cells. **a**) Representative bright field images of iPSCs undergoing retinal differentiation on day 2 (first column, 10x magnification), day 4 (middle column, 25x magnification) and day 25 (last column, 20x magnification). **b**) Immunocytochemical analysis of

bioRxiv preprint doi: https://doi.org/10.1101/288480; this version posted March 25, 2018. The copyright holder for this preprint (which was not certified by peer review) is the author/funder. All rights reserved. No reuse allowed without permission.

SCA7 (top panel) and control (bottom panel) retinal cells showed positive staining for ATXN7 (ATXN7, first column, red), cone-rod homeobox (CRX, middle column, green) and recoverin (RCVRN, last column, red) on day 30 of the differentiation experiment. Nuclei in blue. **c**) qPCR results confirmed the expression of *CRX, PAX6, RCVRN* and *OTX2* in all five lines, compared with the iPSC lines from which they were derived. All levels shown relative to beta actin (ACTB).

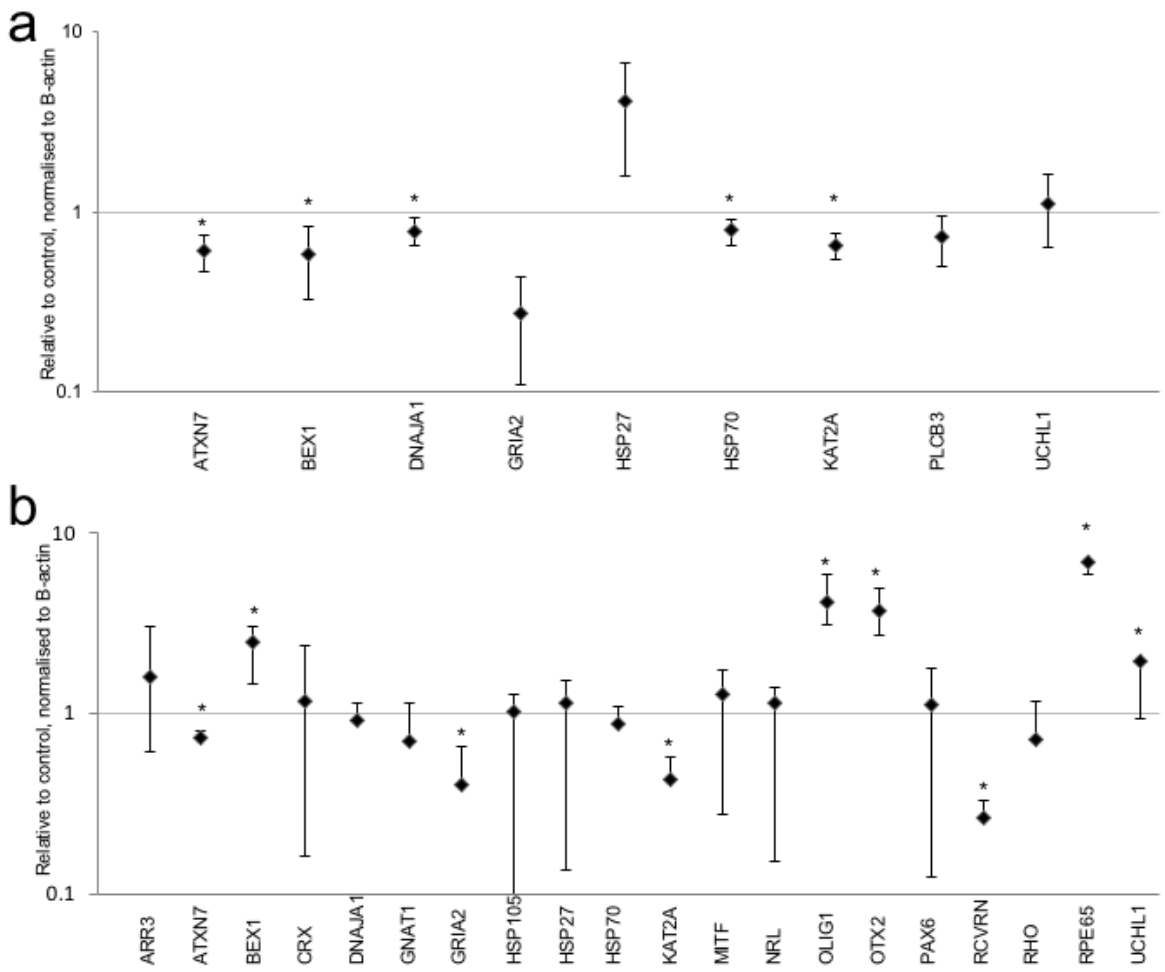

Figure 6: Transcriptional changes in SCA7 iPSC-derived NPCs and retinal cells. **a**) Expression of 9 selected genes in SCA7 patient NPCs (n = 2) shown relative to unaffected control NPCs (n = 2). **b**) Expression of 23 selected genes in SCA7 patient iPSC-derived retinal cells (n=2) shown relative to unaffected control cells (n = 1). All levels shown relative to beta actin (ACTB) and unaffected control cells. *** $p \leq 0.05$.

bioRxiv preprint doi: https://doi.org/10.1101/288480; this version posted March 25, 2018. The copyright holder for this preprint (which was not certified by peer review) is the author/funder. All rights reserved. No reuse allowed without permission.

13. Supplementary Material

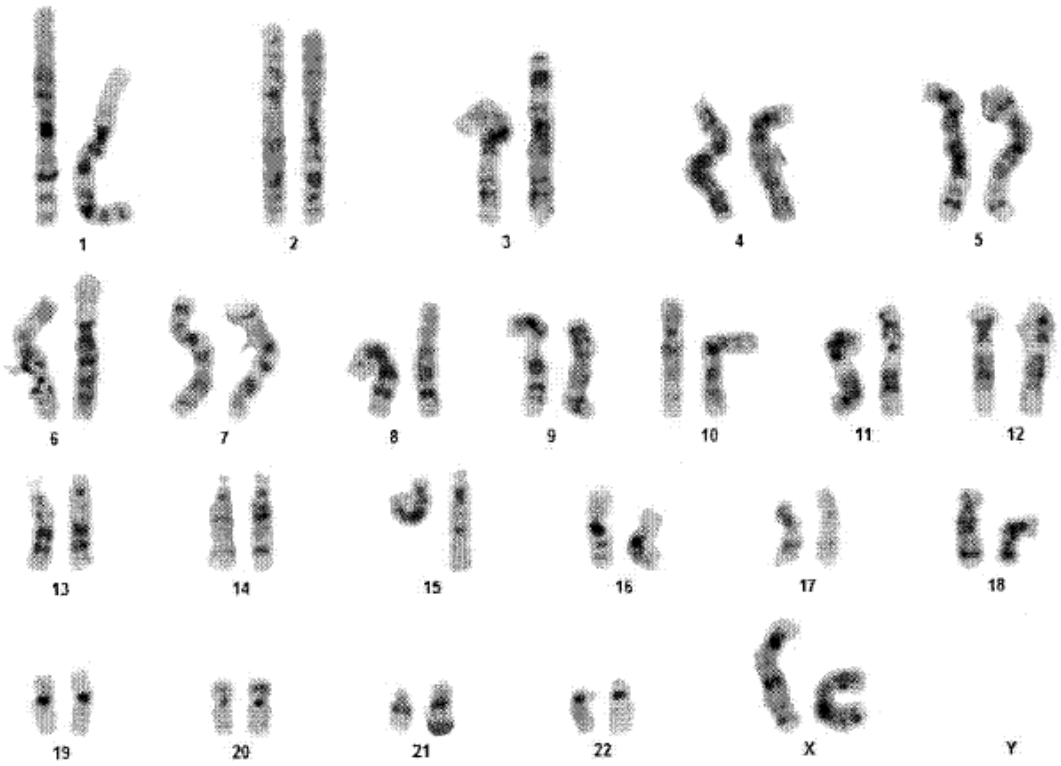

Figure S-1.1: Representative karyogram of an iPSC line, showing no gross structural abnormalities

bioRxiv preprint doi: https://doi.org/10.1101/288480; this version posted March 25, 2018. The copyright holder for this preprint (which was not certified by peer review) is the author/funder. All rights reserved. No reuse allowed without permission.

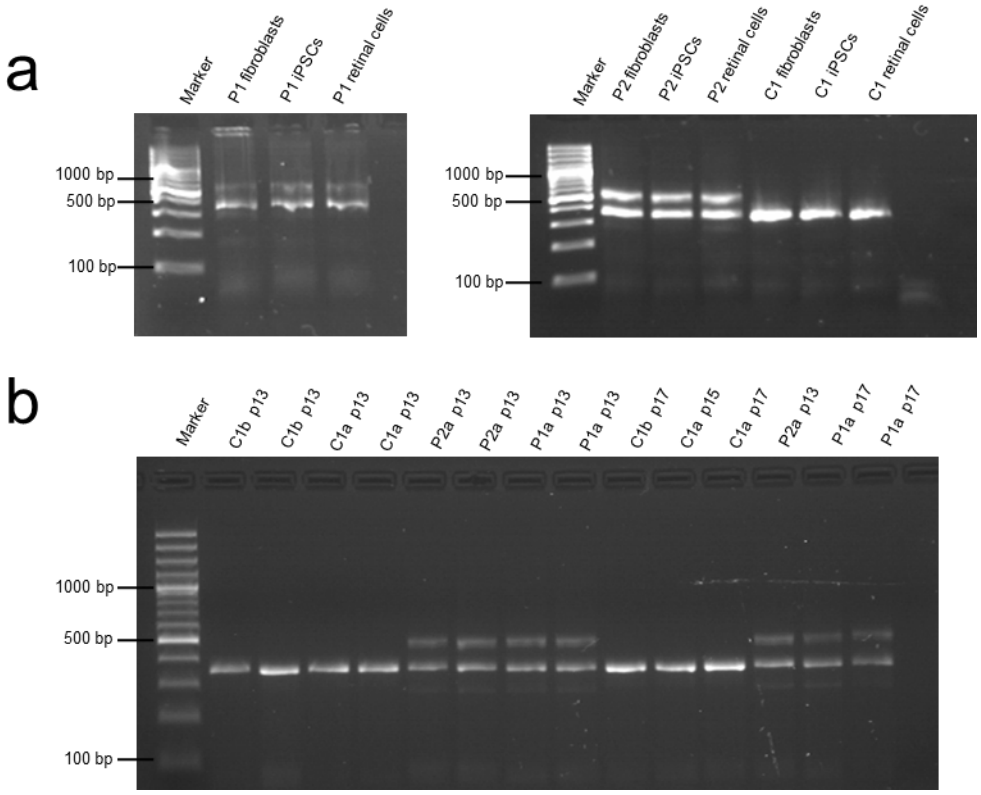

Figure S-1.2 iPSCs, retinal cells (a) and NPCs (b), by semi-quantitative PCR. Samples from all three individuals showed a single band at approximately 355bp, corresponding with a wild-type allele, whilst patient cell lines P1 and P2 showed an additional larger band corresponding to a mutant allele. CAG repeat length in NPCs was evaluated at varying passages (indicated by p13, p15 or p17).

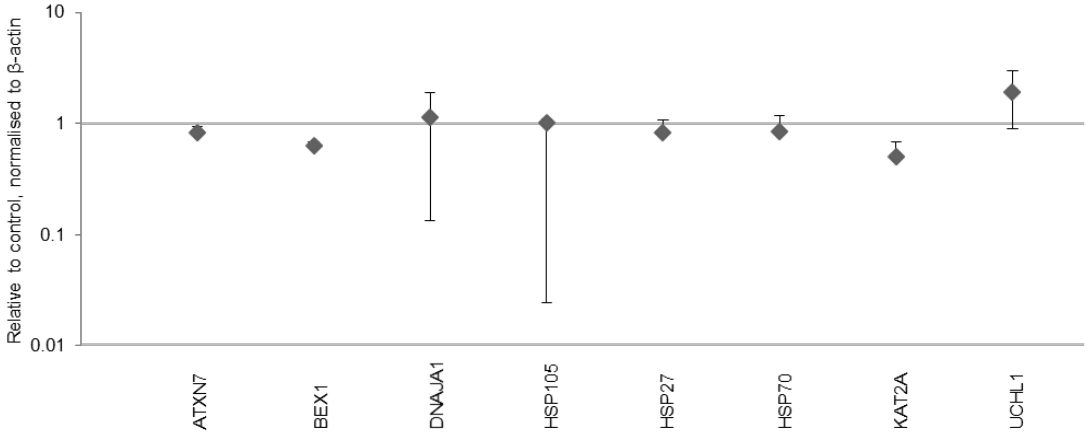

Figure S-1.3: Transcriptional changes in SCA7 patient-derived fibroblasts (n=2), compared to unaffected control fibroblasts (n=1). All levels shown relative to β-actin and unaffected control cells.

Individual code	CAG genotype	Age at diagnosis	Age at biopsy	iPSC codes

bioRxiv preprint doi: https://doi.org/10.1101/288480; this version posted March 25, 2018. The copyright holder for this preprint (which was not certified by peer review) is the author/funder. All rights reserved. No reuse allowed without permission.

P1	10/47	37	50	P1a
P2	10/41	44	44	P2a P2b
C1	10/10	n/a	33	C1a C1b

Table S-1.1: SCA7 patient and unaffected control cell lines, genotypes and ages

Primary antibodies

Antibody	Full name	Species	Supplier	Dilution
AFP	Alpha-fetoprotein	Mouse	Abcam	1:100
ASA	Anti-sarcomeric alpha actinin	Rabbit	Abcam	1:100
ATXN7	Ataxin 7	Rabbit	Thermo Scientific	1:400
CRX	Cone-rod homeobox	Sheep	R&D Systems	1:20
FOXA2	Forkhead box A2	Rabbit	Abcam	1:1000
GABA	γ-aminobutyric acid	Rabbit	Sigma-Aldrich	1:500
GFAP	Glial fibrillary acidic protein	Rabbit	Abcam	1:100
NES	Nestin	Mouse	Abcam	1:1000
NP	Nucleocapsid protein of Sendai virus	Mouse	Gift from Mahito Nakanishi	1:1500
OCT4	POU class 5 homeobox 1	Rabbit	Abcam	1:200
RCVRN	Recoverin	Rabbit	Millipore	1:1000
SMA	Smooth muscle actin	Mouse	Abcam	1:100
TRA-1-60 (PODXL) Alexa-488 conjugated	Podocalyxin like	Mouse	Millipore	1:200
βIII-Tubulin	Tubulin, beta 3 class III	Mouse	Abcam	1:300

Secondary antibodies

Antibody	Dye	Species	Supplier	Dilution
Anti-sheep	Alexa-488	Donkey	Jackson Immunoresearch	1:500
Anti-rabbit	Cy3	Donkey	Jackson Immunoresearch	1:500
Anti-mouse	Alexa-488	Goat	Jackson Immunoresearch	1:500

Table S-1.2: Antibodies for immunocytochemistry

Gene	Primer	Sequence (5' to 3')*
ATXN7	Atxn7 CAG RNA F	HEX-CGAGCTTTCAGAATGCAGC
	Atxn7 CAG RNA F	CACTTCAGGACTGGGCAGAG
B-ACTIN	FORWARD	Proprietary Primer Design UK
	REVERSE	Proprietary Primer Design UK
NANOG	FORWARD	CAGCCCCGATTCTTCCACCAG
	REVERSE	CGGAAGATTCCCAGTCGGGTT
SOX2	FORWARD	GGGAAATGGGAGGGGTGCAAA

bioRxiv preprint doi: https://doi.org/10.1101/288480; this version posted March 25, 2018. The copyright holder for this preprint (which was not certified by peer review) is the author/funder. All rights reserved. No reuse allowed without permission.

	REVERSE	TTGCGTGAGTGTGGATGGGAT
OCT3/4	FORWARD	GACAGGGGGAGGGGAGGAGC
	REVERSE	CTTCCCTCCAACCAGTTGCCC
MITF	FORWARD	TTCACGAGCGTCCTGTATGCAGAT
	REVERSE	TTGCAAAGCAGGATCCATCAAGCC
NRL	FORWARD	GGTCCTAGTCCCAGCTCTTC
	REVERSE	TCGTCCAATCCACATGAGAATTA
OTX2	FORWARD	TGCAGGGGTTCTTCTGTGAT
	REVERSE	AGGGTCAGAGCAATTGACCA
PAX6	FORWARD	CGGAGTGAATCAGCTCGGTG
	REVERSE	CCGCTTATACTGGGCTATTTTGC
RCVRN	FORWARD	CCAGAGCATCTACGCCAAGT
	REVERSE	CACGTCGTAGAGGGAGAAGG
RHO	FORWARD	GTCGATTCCACACGAGCACTG
	REVERSE	CCTCTCTGAATGGATACTTCGTC
RPE65	FORWARD	GCCCTCCTGCACAAGTTTGACTTT
	REVERSE	AGTTGGTCTCTGTGCAAGCGTAGT
ARR3	FORWARD	TCACTTCCAAGTCATCACGG
	REVERSE	GGTGTTGTCCTGGTTGATCC
GNAT1	FORWARD	TAGCTGAGGGGAGTGCAAAT
	REVERSE	CCTCAAAGACTGTGGCCTCT
ATXN7	FORWARD	GCCAGCCGTGAACAATGTC
	REVERSE	TTCCTCCCCGTGCTATTTTCA
BEX1	FORWARD	GGAGGAGACTACAAGGATAGG
	REVERSE	TCCTTTTCTTCATTTTCTTGGTT
DNAJA1	FORWARD	AAAGGAGGAGAACAGGCAATTAA
	REVERSE	TAGGGTTACTGAGAGCTGATGT
GRIA2	FORWARD	CTATGGCATCGCAACACCTAA
	REVERSE	GTCCTTGGCTCCACATTCAC
HSP27	FORWARD	ACGAGCTGACGGTCAAGAC
	REVERSE	GGGGGCAGCGTGTATTTCC
HSP70	FORWARD	ATGGAATCTATAAGCAGGATCT
	REVERSE	CACATACAGAAACTTGATAAGC
HSP105	FORWARD	CCCGTCAGTCATATCATTTGGA
	REVERSE	AATCTTTTGAAGTTAGACACCGTATT
OLIG1	FORWARD	GTTTGGAGAGCTGTATTTAAGACT
	REVERSE	TTCTAAGAAACCCCCAGGATTTA
UCHL1	FORWARD	TGAAGCAGACCATTGGGAAT
	REVERSE	TGTTTCAGAACTGATCCATCCT
PLCB3	FORWARD	CCTTGGAAATCTTTGAGCGGTTC
	REVERSE	ACTTCGTTGAGTCTCGGGTC

Table S-1.3: Primer sequences